Relaxin/insulin-like family peptide receptor 4 (Rxfp4) expressing hypothalamic neurons modulate food intake and preference in mice

Author list – Jo E Lewis[1,*], Orla RM Woodward[1,*], Christopher A Smith[1], Alice E Adriaenssens[1], Lawrence Billing[1], Cheryl Brighton[1], Benjamin U Phillips[2], John A Tadross[1,3], Sarah J Kinston[4], Ernesto Ciabatti[4], Berthold Göttgens[4], Marco Tripodi[5], David Hornigold[6], David Baker[6], Fiona M Gribble[1,#], Frank Reimann[1,#]

Affiliations:

[1]Wellcome Trust – MRC Institute of Metabolic Science Metabolic Research Laboratories, Addenbrooke's Hospital, Hills Road, Cambridge, CB2 0QQ, UK

[2] Department of Physiology, Development and Neuroscience, University of Cambridge, Cambridge, UK.

[3] Department of Pathology, University of Cambridge, Cambridge CB2 1QP, UK

[4] Department of Haematology, Wellcome and MRC Cambridge Stem Cell Institute, University of Cambridge, Cambridge, UK

[5] MRC Laboratory of Molecular Biology, Neurobiology Division, Francis Crick Avenue, Cambridge CB2 0QH, UK

[6] Research and Early Development Cardiovascular, Renal and Metabolism (CVRM), BioPharmaceuticals R&D, AstraZeneca Ltd, Cambridge, UK

* These authors contributed equally to this work.

[#] Corresponding authors – acting correspondence: Frank Reimann (email: fr222@cam.ac.uk)

Abstract

Relaxin/insulin-like-family peptide receptor-4 (RXFP4), the cognate receptor for insulin-like peptide 5 (INSL5), has previously been implicated in feeding behaviour. To explore *Rxfp4* expression and physiology, we generated *Rxfp4*-Cre mice. Whole body chemogenetic activation (Dq) or inhibition (Di) of *Rxfp4*-expressing cells using designer receptors exclusively activated by designer drugs (DREADDs) altered food intake and preference. Potentially underlying this effect, *Rxfp4*-expressing neurons were identified in nodose and dorsal root ganglia and the central nervous system, including the ventromedial hypothalamus (VMH). Single-cell RNA-sequencing defined a cluster of VMH *Rxfp4*-labelled cells expressing *Esr1, Tac1* and *Oxtr*. VMH-restricted activation of *Rxfp4*-expressing (RXFP4^{VMH}) cells using AAV-Dq recapitulated the whole body Dq feeding phenotype. Viral tracing demonstrated RXFP4^{VMH} neural projections to the bed nucleus of the stria terminalis, paraventricular hypothalamus, paraventricular thalamus, central nucleus of the amygdala and parabrachial nucleus. These findings identify hypothalamic RXFP4 signalling as a key regulator of food intake and preference.

Introduction

Relaxin/insulin-like-family peptide receptor-4 (RXFP4) is the cognate receptor for insulin-like peptide 5 (INSL5), a member of the relaxin/insulin-like peptide family and can also be activated by relaxin-3 [1-3]. The primary source of endogenous INSL5 is the distal gut, where it is co-secreted with glucagon-like peptide-1 (GLP-1) and peptide YY (PYY) from enteroendocrine L-cells [4]. Contrasting with GLP-1 and PYY, which exert strong anorexigenic activity, INSL5 seems to be orexigenic [5]. Indeed, *Rxfp4*$^{-/-}$ mice exhibit altered meal patterns and food preference [5] and central infusion of small molecular agonists of RXFP3/RXFP4 increases food intake in rats [6]. Although the physiological role of endogenous INSL5 remains incompletely understood, RXFP4 deserves consideration as a potential target receptor for the manipulation of feeding behaviour.

Expression of *Rxfp4*, a $G_{\alpha i/o}$-coupled G-protein-coupled receptor (GPCR), has previously been identified in several peripheral tissues including the colon, kidney, testes, ovary, heart and liver [7-9]. Its role as the receptor for INSL5 was corroborated by the finding that the orexigenic activity of INSL5 was not observed in *Rxfp4* knockout mice (*Rxfp4*$^{-/-}$) [5]. Relatively little is known, however, about the conditions that might be associated with elevated endogenous INSL5 activity. Increased plasma levels were observed in calorie-restricted mice [5], albeit with the caveat that immuno-assays against endogenous INSL5 are not fully reliable[10]. INSL5 expression was also shown to be higher in germ-free mice and mice treated with broad-spectrum antibiotics, and suppressed by a high fat diet (HFD) [11]. However, *Insl5* knockout mice (*Insl5*$^{-/-}$) do not display an observable feeding phenotype and in some studies pharmacological administration of INSL5 (both native and PEGylated forms) failed to increase food intake in lean and obese mice [11, 12]. Nonetheless, we recently reported a mild orexigenic effect of stimulating INSL5-positive colonic L-cells in mice, revealed upon blockade of the PYY receptor Y2R [13]. Furthermore, an association between *Rxfp4* polymorphisms

and body mass index has been demonstrated in US Caucasian individuals treated with antipsychotic drugs [14].

In this study, we sought to identify and manipulate *Rxfp4*-expressing cells using a newly developed transgenic mouse model in which Cre-recombinase expression is driven by the *Rxfp4* promoter (*Rxfp4*-Cre). We detected *Rxfp4* expression in several nuclei in the central nervous system (CNS) previously implicated in food intake control. *Rxfp4*-expressing cells were functionally manipulated using Cre-dependent expression of designer receptors exclusively activated by designer drugs (DREADDs). Activation in all *Rxfp4*-expressing cells of a Gi-coupled DREADD (Di), which should mimic the physiology of INSL5-RXFP4 signalling, increased highly palatable food intake. Conversely, activation of a Gq-coupled DREADD (Dq) in *Rxfp4* cells resulted in reduced intake of highly palatable meals. Similar effects were seen when the ventromedial hypothalamic population of *Rxfp4*-expressing neurons was selectively targeted with rAAV-Dq. This cell population was further characterised by single-cell RNA sequencing (scRNA-seq) and projection mapping, establishing RXFP4 as a potential target for the manipulation of food preference.

Results

To investigate a possible role of *Rxfp4*-expressing cells in feeding control, we generated a new BAC transgenic mouse (*Rxfp4*-Cre) model in which Cre-recombinase is expressed under the control of the *Rxfp4*-promoter (Fig. 1a). By crossing *Rxfp4*-Cre mice with fluorescent protein reporter mice (e.g. Rosa26 fxSTOPfx-EYFP (RXFP4^{EYFP})) (Fig. 1b) we observed *Rxfp4* dependent expression in the colon (Fig 1c), consistent with previous reports, however, expression seemed restricted to enteroendocrine cells, particularly serotonin producing enterochromaffin (EC)-cells (Supp. Fig. 1a), rather than, as previously suggested [5], enteric neurons (Suppl. Fig.1d). We observed *Rxfp4*-expression in vagal and spinal afferent neurons in nodose and dorsal root ganglia (DRG) (Suppl. Fig. 1e,f), and readily detected reporter expression in the central nervous system (CNS) (Suppl. Fig. 2). Within the CNS we observed reporter expression in the accessory olfactory bulb, septofimbrial nucleus, retrosplenial cortex and the mammillary body medial and lateral parts, as well as in a lower density of cells in the substantia innominata, cortical and central amygdala, periaqueductal grey, and spinal trigeminal tract of the hindbrain (Suppl. Fig 2). Examination of RXFP4^{GCaMP3} mice clearly revealed transgene expression in the ventrolateral part of the ventromedial hypothalamus (VMHvl) extending into the adjacent tuberal nucleus (TN) (Fig. 1d,e), despite our previously reported failure to amplify *Rxfp4* from hypothalamic cDNA by RT-PCR [5]. In the VMHvl, co-staining with NeuN demonstrated GFP expression in mature RXFP4 positive neurons (Fig. 1f). Active transcription of *Rxfp4* mRNA in the adult mouse hypothalamus was confirmed by RNAscope (Fig.1g,h) and RT-qPCR (Suppl. Fig. 1i).

Given the observed peripheral and central neuronal expression of *Rxfp4* and the previously reported altered feeding patterns and macronutrient preferences in *Rxfp4* knock-out mice [5], we investigated the effects of DREADD activation in *Rxfp4*-expressing cells. Initially we used a whole-body hM4Di Cre-reporter (RXFP4$^{wb\text{-}Di}$) to mimic the established RXFP4-signalling via pertussis-toxin sensitive Gi pathways [2] (Fig. 2a).

During the light phase, activation of Di in *Rxfp4*-expressing cells using CNO had no measurable effect on food intake in mice eating standard chow (Fig. 2b). However, when animals were adapted to the appearance of a high fat diet (HFD) or a highly palatable liquid Ensure test meal (HPM), during the light phase, CNO application resulted in increased food intake (Fig. 2c,d). To investigate this further, we gave mice housed in metabolic cages the choice between standard chow and HFD. CNO injection during the light phase significantly increased HFD but not chow intake in RXFP4$^{wb\text{-}Di}$ mice (Fig. 2e). This effect was transient (Fig. 2f), consistent with the pharmacokinetics of CNO [15], and occurred without any significant differences in ambulatory activity or energy expenditure compared to the saline cross-over control (Suppl. Fig. 3a,b).

We next investigated the effects of whole-body hM3Dq Cre-reporter activation in *Rxfp4*-expressing cells (RXFP4$^{wb\text{-}Dq}$) (Fig. 3a). Similar to the results in RXFP4$^{wb\text{-}Di}$ mice, activation of Dq in *Rxfp4*-expressing cells with CNO had no measurable effect on ad lib fed mice offered a standard chow, which was tested at the onset of the dark phase when mice are normally highly motivated to feed (Fig. 3b). However, when RXFP4$^{wb\text{-}Dq}$ animals were adapted to the appearance of HFD or a HPM at the onset of the dark phase, activation of Dq expressing cells with CNO resulted in a marked reduction in food intake (Fig 3. c,d). These results were consolidated in ad lib fed animals in metabolic cages with parallel access to standard chow and HFD. RXFP4$^{wb\text{-}Dq}$ activation in ad lib fed animals at the onset of the dark phase, had no effect on standard chow intake, but significantly and transiently reduced HFD consumption (Fig 3. e,f). RXFP4$^{wb\text{-}Dq}$ activation also attenuated the increase in energy expenditure associated with the onset of the dark phase, however, there was no effect on ambulatory activity (Suppl. Fig. 3c,d).

To probe whether *Rxfp4*-expressing cells play a role in the motivational aspects of feeding, we calorically restricted male RXFP4$^{wb\text{-}Dq}$ animals to 95% body weight and placed them in operant chambers. Mice were either tested with a fixed ratio (FR) schedule, requiring 5 nose pokes to release a food reward, or a

progressive ratio (PR) schedule requiring increasing number of nose pokes for each subsequently earned reward (in this case, +4, i.e. 1, 5, 9, 13, etc). RXFP4$^{wb\text{-}Dq}$ mice treated with CNO completed fewer attempts under FR to earn individual Ensure meals/rewards (Fig. 3g). Under a PR schedule, they exhibited a reduced breakpoint – i.e. CNO-treated mice stopped working for the HPM-reward at lower ratios than when receiving vehicle treatment (Fig. 3h). In an effort related choice (ERC) paradigm, where animals had the choice of working for a HPM (FR8, liquid Ensure) or consuming freely available standard chow, CNO treatment reduced HPM consumption (Fig. 3i). However, animals consumed similar amounts of standard chow and displayed otherwise normal behaviour (supplementary video 1), suggesting that activation of *Rxfp4*-expressing cells reduced motivation for the HPM rather than inducing generalised malaise.

Rxfp4-expressing cells were identified in the VMHvl (Fig. 1d,e), a central hub for the regulation of energy balance and integration of diverse nutritionally regulated hormonal and synaptic inputs, as well as in the adjacent TN previously implicated in feeding behaviour [16, 17]. To assess whether this *Rxfp4*-expressing population is involved in the feeding phenotype observed in RXFP4$^{wb\text{-}Dq}$ mice, the effect of acute chemogenetic manipulation of *Rxfp4*-expressing VMHvl cell activity on food intake was investigated. Male *Rxfp4*-Cre mice received bilateral VMHvl injections of Cre-dependent hM3Dq-expressing rAAVs (AAV-hSyn-DIO-hM3D(G)q-mCherry) designed to preferentially target neurons, to produce RXFP4^{VMHDq} mice (Fig. 4a). Targeting efficiency was subsequently determined by immunohistochemistry (Fig. 4b). All included mice demonstrated robust transduction that was limited to the target region; one mouse, due to misplacement of the cannula and subsequent infusion, demonstrated off-target expression i.e., expression outside the VMHvl. This mouse was excluded from the analysis. The effect of chemogenetic activation of this cell population on food intake was studied in a crossover design. In chow fed mice, and in line with RXFP4$^{wb\text{-}Dq}$ animals, CNO treatment of RXFP4^{VMHDq} mice had no effect on standard chow intake at the onset of the dark phase (Fig. 4c). When animals were habituated to the appearance of a HFD or HPM at the onset of the dark phase, CNO resulted in a significant reduction in food intake (Fig. 4d,e).

When offered HFD and chow diet in parallel in metabolic cages, CNO significantly reduced intake of the HFD whilst intake of standard chow was not altered, resulting in an overall reduced caloric intake (Fig. 4f). As seen with RXFP4$^{wb\text{-}Dq}$ animals, this was a transient effect, which was no longer apparent 2 hours post administration of CNO (Fig. 4g). CNO had no effect on energy expenditure or ambulatory activity in these RXFP4^{VMHDq} animals (Suppl. Fig. 3e,f). RXFP4^{VMHDq} mice were subsequently offered water and 2% sucrose in parallel in metabolic cages, and although animals preferentially consumed 2% sucrose, CNO did not affect intake (Suppl. Fig. 4a,b).

We subsequently generated a single cell resolution transcriptomic profile of *Rxfp4*-expressing cells in the hypothalamus. Fluorescent cell populations from the hypothalamus of RXFP4^{EYFP} mice were purified by FACS and their transcriptomes analysed by scRNA-Seq. Graph-based clustering analysis revealed that hypothalamic *Rxfp4*-expressing cells separate into five populations (Fig. 5a). Cluster identities were assigned based on the expression patterns of canonical cell-type markers, with macrophages (*Mrc1*, *Mgl2*), microglia (*Tmem119*, *Siglech*, *P2ry12*), neuronal cells (*Snap25, Tubb3, Elavl2*), ependymocytes (*Ccdc153*, *Hdc*) and endothelial cells (*Dcn*, *Hspg2*) representing distinct clusters (Fig. 5b). As hypothalamic neurons are known to modulate feeding behaviour, we analysed the neuronal cluster in more detail, identifying seven subclusters (Fig. 5c). *Rxfp4*-positive neurons expressed markers for both GABAergic (*Slc32a1*) and glutamatergic (*Slc17a6*) cells (Fig 5d). Cluster 1 was enriched in markers previously associated with an estrogen receptor (*Esr1*)-positive VMHvl neuronal population [18, 19], including preprotachykinin-1 (*Tac-1*), oxytocin receptor (*Oxtr*), cholecystokinin receptor A (*Cckar*), melanocortin 4 receptor (*Mc4r*) and neuromedin U receptor 2 (*Nmur2*) (Fig 5d), suggesting crosstalk with known food regulatory networks. Receptors for other established feeding-neuromodulators, like glucagon-like peptide-1 receptor (*Glp1r*) and cholecystokinin receptor B (*Cckbr*), were preferentially expressed in cluster 6 (Fig 5d).

Finally, we aimed to establish the neuronal circuitry surrounding *Rxfp4*-expressing cells in the VMHvl. We performed viral anterograde and retrograde projection mapping by stereotactically injecting Cre-dependent AAV8-ChR2-mCherry [20] and AVV2-TVAeGFP-oG/ Rab-ΔG-EnvA-mCherry [21], respectively into the VMH of *Rxfp4*-Cre mice. The anterograde axonal transport of the ChR2-mCherry fusion revealed robust RXFP4^{VMH} projections to multiple regions including the bed nucleus of the stria terminalis (BNST), preoptic area (POA) and anteroventral periventricular nucleus (AVPV), arcuate nucleus (ARC), paraventricular hypothalamus (PVH), central nucleus of the amygdala (CeA), periaqueductal gray (PAG, dorsomedial and lateral) and lateral parabrachial nucleus (LPBN) (Fig. 6a-c, Suppl. Fig. 6). The retrograde monosynaptic transport of Rab-mCherry labelled inputs from several nuclei established in feeding regulation, including the ARC and PVH (Fig. 6d-f). The neuronal circuitry surrounding *Rxfp4*-expressing cells is summarised in Fig. 6g.

Discussion

The *Rxfp4*-Cre mouse model generated in this study has enabled the identification of peripheral and central *Rxpf4*-expressing cells, and aided the transcriptomic, functional and anatomical characterisation of a hypothalamic *Rxfp4*-expressing neuronal population. We show that *Rxfp4* is expressed in key feeding centres of the brain, including neurons of the VMHvl. Chemogenetic activation of this population suppressed HFD and HPM intake, reflecting their position in brain circuits previously implicated in homeostatic and hedonic regulation of food intake. These data identify hypothalamic RXFP4 signalling as a key regulator of food intake and preference.

Rxfp4 expression has been difficult to localise due to seemingly low mRNA expression levels and the lack of suitable verified antibodies. *Rxfp4* expression has previously been reported in the colon [5] and in enteroendocrine tumor cell lines [22, 23] and here we demonstrate *Rxfp4*-reporter expression in enterochromaffin (EC)-cells by immunohistochemistry (Suppl. Fig. 1a). Consistent with EC-expression, FACS sorted colonic RXFP4^{EYFP} cells were enriched for *Tph1* mRNA, the first enzyme in the serotonin biosynthesis pathway and for *Rxfp4* itself, confirming active receptor transcription (Suppl. Fig. 1b,c). Although previous *in situ* hybridization suggested expression in the enteric nervous system (ENS) [5], we did not observe reporter expression in enteric neurons, but were able to detect expression in afferent neurons innervating the colon. We also did not detect *Rxfp4*-reporter expression in the endocrine pancreas (Suppl. Fig. 1g,h), suggesting RXFP4 is unlikely to play a physiological relevant role in pancreatic hormone secretion. This contradicts reports of INSL5 stimulating insulin secretion [24], but is in keeping with a lack of *Rxfp4* mRNA detection in mouse pancreatic islet cells [25] and our failure to observe any effect of CNO on glucose tolerance in lean and diet-induced obese RXFP4$^{wb\text{-}Dq}$ and RXFP4$^{wb\text{-}Di}$ mice (Suppl. Fig. 7). In contrast to our previous report [5], we detected *Rxfp4* mRNA in the hypothalamus (Suppl. Fig. 1i) and found substantial reporter expression in multiple brain regions with distinct *Rxfp4*-expressing cell populations in the accessory olfactory bulb, RSC, VMHvl, and mammillary body (Fig. 1d, Suppl. Fig. 2). This

could, in principle, be lineage tracing events from precursor cells. However, the activation of Cre-reporter rAAV-constructs when stereotactically injected into the adult VMH is consistent with active *Rxfp4*-promoter activity driving *Cre*-expression, and the detection of *Rxfp4* mRNA by RT-qPCR and RNAscope further consolidate active *Rxfp4* expression in the adult mouse brain (Fig. 1g,h, Suppl. Fig. 1i).

Inhibition of *Rxfp4*-expressing cells via Di acutely increased intake of both a HFD and a HPM in the home cage and when animals were offered a choice of standard laboratory chow and HFD in metabolic cages, without altering energy expenditure and activity in both male and female mice (Fig 2, Suppl. Fig 3a,b). This is consistent with our previous demonstration that INSL5 administration increased food intake [5, 13], as activation of Di receptors should at least in part mimic the $G\alpha_{i/o}$ coupling of RXFP4 [2]. Other relaxin family peptide receptors have also been implicated in energy homeostasis, with dual agonists of RXFP3/4 increasing food intake in rats following acute central administration [6]. The increase in food intake observed in $RXFP4^{wb\text{-}Di}$ mice was, however, modest and more subtle than that reported for $AGRP^{Dq}$ animals, which showed, at least transiently, a phenotype even on standard chow [26].

Activation rather than inhibition of *Rxfp4*-expressing neurons with Dq produced a robust and reproducible suppression of food intake. We particularly focused on a central *Rxfp4*-expressing population in the VMHvl, which is a region previously implicated in feeding and energy expenditure [16, 17]. However, the adjacent TN, which has also been implicated in feeding behaviour [17], may have also been targeted during stereotactic injections, as disparities between current mouse brain atlases on the exact location of the TN make it difficult to distinguish from the VMHvl. The *Rxfp4*-expressing population we targeted is therefore best described as $RXFP4^{VMH}$. Targeting this population with an rAAV-Dq reporter recapitulated the findings with the whole body-Dq reporter (Fig. 4). Whilst any of the identified *Rxfp4*-expression sites could participate in the feeding phenotype of the global DREADD reporter mice, the VMH-selective rAAV-Dq reporter phenotype indicates that this hypothalamic population is at least in part underlying the observed

anorexigenic effects in the RXFP4$^{wb\text{-}Dq}$ model. However, an additional peripheral signalling pathway involving afferent sensory fibres cannot be excluded, given the robust *Rxfp4* mRNA expression and labelling in RXFP4^{EYFP} mice in somata located in dorsal root and nodose ganglia.

Our data suggest that activation of *Rxfp4*-expressing cells in the VMH suppresses the consumption and drive to work for calorie dense HFD and HPM food. The importance of the VMH in the regulation of feeding and metabolism has been disputed (reviewed in [27]). Initial studies suggested the VMH might be a "satiety centre", as VMH-lesioned rats, particularly females, over-consumed when fed ad libitum [28], despite being seemingly less willing to work for food on a fixed ratio lever-pressing paradigm [29]. The observed hyperphagia has subsequently, however, been linked to additional damage to adjacent hypothalamic structures (see King 2006[27] for discussion), whilst the reduced motivation was not observed when rats were trained pre-operatively, suggesting that the VMH lesion altered the "trainability" rather than feeding motivation [27, 30]. Lesioning studies, whilst informative, lack cellular precision and damage neural connections to other feeding centres within the brain. More recent work employing immunohistochemistry, RNA sequencing, chemogenetic techniques and neuronal projection mapping, has demonstrated that the VMH consists of anatomical subdivisions made up of heterogeneous but distinct cell populations[18, 31, 32]. Functional studies suggest neurons in the central and dorsomedial VMH regulate feeding, energy expenditure and glucose homeostasis [33, 34], while the VMHvl is more frequently implicated in the control of social and sexual behaviours[32, 35, 36]. However, several studies have demonstrated the involvement of VMHvl neurons in energy expenditure and feeding behaviour [16, 37]. Increases in physical activity have been observed following chemogenetic activation of NK2 homeobox transcription factor 1 (*Nkx2-1*)-expressing neurons in the VMHvl of female rats, while knockout of *Nkx2-1* in the VMHvl leads to decreased physical activity and thermogenesis [38]. Furthermore, chemogenetic activation of *Esr1*-expressing VMHvl neurons was found to stimulate physical activity and thermogenesis in both sexes [19]. *Esr1* signalling in the VMHvl was previously demonstrated to influence food intake, energy

expenditure and glucose tolerance as VMHvl-restricted knockdown of *Esr1* resulted in increased food intake, decreased physical activity and thermogenesis, reduced glucose tolerance and obesity in female rats [16]. By contrast, activation of *Rxfp4*-expressing cells in the VMHvl in RXFP4^{VMHDq} mice reduced HFD and HPM intake but had no effect on chow intake, energy expenditure or ambulatory activity (Fig. 4, Suppl. Fig. 3e,f). This suggests that *Rxfp4*-expressing neurons comprise a unique VMHvl population modulating the rewarding aspects of food rather than the homeostatic food intake or energy expenditure responses observed during chemogenetic manipulation of other VMHvl populations.

To identify whether hypothalamic *Rxfp4*-expressing cells could be assigned to known neural networks we performed scRNA-Seq which revealed substantial cellular heterogeneity. Although some cells will have been lost and some genes may have exhibited altered expression during the cell dissociation and sorting process, the results allowed us to cluster *Rxfp4*-expressing cells into several subpopulations each characterised by a profile of canonical cell-type marker genes (Fig. 5a,b). Our identification of *Rxfp4* in microglia, ependymocytes and endothelial cells that potentially constitute the blood brain barrier, raises the possibility that INSL5 may exert effects on non-neuronal cells [39]. Clustering of the *Rxfp4*-expressing neuronal population illustrated a predominance of glutamatergic neurons with few GABAergic clusters (Fig 5d). Cluster 6 is of note given the expression of *Glp1r*, *Cckbr*, *Sstr1* and *Sstr2*, suggesting an overlap with other known appetite-modulating gut peptide receptors. The cocaine- and amphetamine-regulated transcript (*Cartpt*), expressed in cluster 3, and cannabinoid receptor 1 (Cnr1), expressed in clusters 1, 4 and 5, (Suppl. Fig. 5) are also implicated in energy homeostasis[40, 41]. Cluster 1 displays markers of a VMHvl *Esr1* population (*Esr1, Pgr, Tac1, Cckar, Rprm* and *Oxtr*) previously associated with food intake and energy expenditure[16, 18, 19]. Whilst there is clearly co-expression of *Rxfp4* and *Esr1* expression in the VMHvl, chemogenetic activation of RXFP4^{VMHDq} neurons did not result in increased energy expenditure or ambulatory activity, contrasting with the described Esr1^{VMHDq} phenotype[19]. An important role of VMHvl *Rxfp4*-expressing cells in feeding regulation is further suggested by the co-expression of the neuropeptide

receptors *Mc4r* and *Nmur2.* MC4R activation has been linked to suppressed food intake through regulation of *Bdnf* expression in the VMH [42] – *Bdnf* is co-expressed in cluster 1 neurons in our dataset (Fig. 5d). Acute administration of NMUR2 agonists have been shown to decrease feeding, with one agonist being somewhat selective to HFD intake regulation [43], mirroring RXFP4^{VMHDq} cell activation (Fig 4). scRNA-Seq has previously revealed heterogeneous VMHvl neuronal populations which can be broadly categorised into three subdivisions based on the expression of *Esr1, Dlk1* (Delta-like homolog 1) or *Satb2* [18]. In accordance with this dataset, we identified *Esr1* in cluster 1, as described above, and we also observed *Dlk1* expression in the GABAergic clusters 4 and 5 (Fig. 5d). These clusters may reflect VMHvl *Dlk1* expression as observed by Kim et al., but may also indicate other hypothalamic *Rxfp4*-expressing neurons given the relatively widespread expression of *Dlk1* in the hypothalamus. The role of hypothalamic *Dlk1* expression in energy homeostasis has not been functionally explored, however this gene has been implicated in obesity in mice and humans [44, 45]. We detected very low levels of *Satb2* in our hypothalamic *Rxfp4*-expressing cells (Suppl. Fig. 4) suggesting limited overlap between *Rxfp4* and *Satb2* populations.

Mapping of the retrograde inputs to and anterograde projections from RXFP4^{VMH} cells revealed a distinct neural circuitry surrounding this hypothalamic population. Monosynaptic inputs were labelled predominantly from brain regions involved in homeostatic regulation of food intake such as the ARC, PVH and LHA (Fig. 6f). Within the ARC, two populations of neurons have been intensely studied with regards to feeding regulation: pro-opiomelanocortin (POMC)/cocaine- and amphetamine-regulated transcript (CART)-expressing neurons inhibit food intake while Agouti-Related Peptide (AgRP)/neuropeptide Y (NPY)-expressing neurons stimulate food intake. These neurons integrate nutritional and hormonal signals from the periphery, detected due to the leaky blood brain barrier in the adjacent median eminence, and send projections to multiple brain regions including the VMH [46]. Given the co-expression of *Mc4r* in the RXFP4^{VMHvl} neurons it seems likely that POMC neurons are part of this ARC innervation of RXFP4^{VMHvl} neurons, even though the VMH is not thought to be the main target of arcuate POMC projections [47].

RXFP4^{VMH} cells predominantly project onto regions associated with reward and motivation-related behaviours (Fig. 6c, Suppl. Fig. 6) such as the BNST, POA, CeA, paraventricular thalamic nucleus (PVT) and ventral tegmental area (VTA) [48-50], potentially underlying our finding that chemogenetic activation of *Rxfp4*-expressing cells in RXFP4$^{wb\text{-}Dq}$ mice reduced an animal's drive to seek out and work for a highly palatable food reward (Fig 3g-i). Taken together, these data suggest that *Rxfp4*-expressing cells influence motivation and reward-related behaviour, potentially via regulation of central reward signalling pathways. RXFP4^{VMH} cells also send projections to the PAG and LPBN, two integration sites responsible for relaying sensory information between the forebrain and hindbrain and coordinating behaviour in response to various stimuli including metabolic, gustatory and nociceptive inputs [51-53]. This RXFP4^{VMH} projection map aligns with previously identified projection regions from the VMHvl and SST-expressing cells in the TN [17, 54]. Given the difficultly in defining the boundary between the VMHvl and TN, it is possible that some *Rxfp4*-expressing cells in the TN were transfected by the viral vectors and acted as starter cells in these tracing experiments. Interestingly, all retrograde-labelled input regions also received projections from RXFP4^{VMH} cells suggesting a high level of bidirectional connectivity within the RXFP4^{VMH} signalling network (Fig. 6g). Similar bidirectional connectivity has been shown for an *Esr1*+ve VMHvl population [54]. The RXFP4^{VMH} neural network established in this study suggests these cells may integrate metabolic and nutritional cues either directly or via other hypothalamic regions and regulate the reward system to influence ingestive behaviours. The low number of RXFP4^{VMH} input regions compared to projection regions suggests these cells may comprise an early node in this network.

We recognise several limitations to this study. First, the exact classification of *Rxfp4*-expressing brain regions is difficult given the disparities between current brain atlases. We defined an *Rxfp4*-expressing population in the VMHvl based on anatomical location and mRNA expression profile. However, the inexact nature of stereotactic injections may have resulted in additional targeting of neurons in adjacent LHA and TN regions, which may have contributed to the food intake phenotype of RXFP4^{VMHDq} mice. Although we

have shown that chemogenetic manipulation of *Rxfp4*-expressing cells regulates food intake and food preference, this technique may trigger supraphysiological responses in target cells, so we cannot conclude that similar changes in food intake behaviour would be triggered by physiological activation of RXFP4. The VMHvl is also a sexually dimorphic brain region with activation of different subpopulations giving divergent responses in males and females [37, 38]. While the operant conditioning and RXFP4^{VMHDq} experiments in the present study were only conducted in males, we did not observe sex differences in *Rxfp4*-Cre reporter expression profiles, whole body DREADD activation phenotypes or in RXFP4^{VMH} projection mapping, so we do not believe RXFP4 action to be strongly sexually dimorphic. We also cannot be certain whether endogenous INSL5 acts on *Rxfp4*-expressing cells in the brain to regulate central RXFP4 activity. We have previously been unable to identify *Insl5*-expressing cells in the mouse brain [13] and there is no evidence that INSL5 can cross the blood brain barrier. However, relaxin-3 also activates RXFP4 [2], is expressed in the mouse brain and is orexigenic [55], hence it is possible that relaxin-3, rather than INSL5, is involved in central RXFP4 action. This study has illustrated the neuronal network of RXFP4^{VMH} cells using viral tracing techniques which have some limitations. In the retrograde tracing experiments, it was difficult to detect AAV-GFP immunoreactive cells, making it hard to confirm the exact starter cells in this experiment. Although mCherry-positive cell bodies identified in the adjacent regions, ARC and DMH, could theoretically be starter cells rather than input regions, this seems unlikely based on the small volume of virus injected. Furthermore, while the ChR2-mCherry construct is preferentially targeted to axon terminals, it is possible that some of the mCherry-labelled fibres in adjacent regions, such as the ARC, are in fact dendrites [56] which may underlie our inability to detect retrograde-only labelled regions. Finally, in these tracing experiments we did not detect projections to regions very far from the target region, such as in the hindbrain. This may reflect a lack of very long-range projections from *Rxfp4*-expressing neurons but may also be due to a low concentration of ChR2-mCherry in axon terminals very far from the cell body [56]. Nevertheless, we have been able to identify distinct regions that project onto and receive projections

from *Rxfp4*-expressing cells in the VMH that connect these cells to known feeding-related neural networks.

In summary, we have characterised a previously unrecognised population of ventromedial hypothalamic cells that express *Rxfp4* in mice, demonstrated that their acute activation in males reduces HFD/HPM intake without affecting chow intake or changes in energy expenditure, and identified projections in homeostatic and hedonic feeding centres in the CNS. Together, these findings suggest *Rxfp4*-expressing VMHvl-neurons are key modulators of food preference.

Methods

Animals

All experiments were performed under the UK Home Office project licences 70/7824 and PE50F6065 in accordance with the UK Animals (Scientific Procedures) Act, 1986 and approved by the University of Cambridge Animal Welfare and Ethical Review Body. All mice were from a C57BL/6 background and were group-housed and maintained in individual ventilated cages with standard bedding and enrichment in a temperature and humidity controlled room on a 12h light:dark cycle (lights on 7:00) with ad libitum (ad lib) access to food (Scientific Animal Food Engineering) and water unless otherwise stated. Groups were randomised by body weight and the researcher was blinded to treatment.

Mouse models

To express Cre recombinase under the control of the *Rxfp4* promoter, we replaced the sequence between the start codon and the stop codon in the single coding exon of *Rxfp4* in the murine-based BAC RP24-72I4 (Children's Hospital Oakland Research Institute) with iCre [57] sequence using Red/ET recombination technology (GeneBridges) (Fig 1A). The resulting BAC was used to create BAC-transgenic mice – of four initial founders, two passed the transgene to their offspring; both resulting lines showed similar Cre-

reporter expression and one line, Rxfp4-73, was used throughout this manuscript (see Suppl. methods 1 for further information). Several Cre-reporter transgenes, in which expression is only activated after removal of a fxSTOPfx cassette, were used, resulting in expression of EYFP [58], Dq , Di [59], GCaMP3 [60], or tdRFP [61], respectively.

Viral injections

Viral injections were performed in male and female *Rxfp4*-Cre mice aged between 9 and 16 weeks. The surgical procedure was performed under isoflurane, with all animals receiving Metacam prior to surgery. Mice were stereotactically implanted with a guide cannula (Plastics One) positioned 1mm above the VMH (A/P: -1.7 mm, D/V: -4.5 mm, M/L: +/- 0.75 mm from bregma). Bevelled stainless steel injectors (33 gauge, Plastics One) extending 1mm from the tip of the guide were used for injections. For phenotyping experiments, 200nL AAV-hM3D(G)q-mCherry (Addgene 44361-AAV8, $4x10^{12}$ vg/mL) was injected bilaterally at 50nl/min and mice were allowed 2 weeks recovery prior to testing. For anterograde viral tracing experiments, 200 nL AAV-DIO-ChR2-mCherry (Addgene, 20297-AAV8, 1.9×10^{13} vg/ml) was injected unilaterally at 75 nL/min. Mice were culled three weeks after injection. For retrograde viral tracing experiments, AVV2-FLEX-TVAeGFP-2A-oG (AAV2-TVAeGFP-oG) and Rabies-ΔG-EnvA-mCherry (Rab-ΔG-EnvA-mCherry) viruses were generated by Ernesto Ciabatti (MRC Laboratory of Molecular Biology, Cambridge). Mice were injected unilaterally with 200 nL AVV2-TVAeGFP-oG ($1x10^{12}$ vg/mL) at 75 nL/min followed by 500 nL Rab-ΔG-EnvA-mCherry ($2x10^{9}$ iu/mL) at 75 nL/min three weeks later. Mice were culled seven days after the second injection.

Food intake

Food intake studies were performed in a cross-over manner, on age-matched groups, a minimum of 72 hours apart. For experiments assessing the effect of global RXFP4 Di and Dq activation, animals were singly housed prior to the experiment. Mice were administered 1mg/kg CNO (Sigma) or an equivalent volume

of vehicle containing a matched concentration of DMSO. For light phase activation, animals were injected with vehicle or CNO at 11:00 (± 30mins) following a 2h fast. Food was weighed at 1h post-injection. For dark phase activation, animals were injected with vehicle or CNO at 19:00 at the onset of the dark phase following a 2h fast. Food was weighed at 1h post-injection. In trials with a high fat diet (HFD) and a highly palatable meal (HPM, liquid Ensure, Abbott Laboratories, 353-3601), mice were habituated to the appearance of the test meal (5 days per week) for two weeks prior to testing.

Operant chambers

Twelve male RXFP4$^{wb\text{-}Dq}$ mice (weighed 3 times weekly) were food restricted to maintain 95% body weight for two weeks prior to training and testing in standard mouse Bussey-Saksida touchscreen chambers (Campden Instruments Ltd, Loughborough, UK). Training and testing procedures were conducted as previously described [62]. Briefly, mice were trained to touchscreen for reward (the HPM, 20 µL) under a fixed ratio (FR) schedule for 2 weeks, progressing from FR1 to FR5 (training deemed successful when animal earnt 30 rewards within 1 hour), followed by testing. Mice then progressed to progressive ratio (PR, increment +4 i.e. 1, 5, 9, 13, etc), where the breakpoint was defined as the last reward earned before 5 minutes elapsed without operant response. Following testing of the breakpoint, mice progressed to the effort related choice schedule (ERC) - mice were trained on FR8, with the addition of standard chow to the operant arena. Once animals successfully earned 30 rewards within 60 minutes, testing was undertaken. The 60-minute training and testing sessions took place at the same time each day (between 10:00-13:00).

Metabolic cages

Animals were acclimated to metabolic cages prior to study and data collection. Oxygen consumption and carbon dioxide production were determined using an indirect calorimetry system (Promethion, Sable

Systems, Las Vegas, NV). The system consisted of 8 metabolic cages (similar to home cages), equipped with water bottles and food hoppers connected to load cells for continuous monitoring housed in a temperature and humidity-controlled cabinet. The respiratory exchange ratio (RER) and energy expenditure (via the Weir equation) were calculated, whilst ambulatory activity was determined simultaneously. Raw data was processed using ExpeData (Sable Systems). Animals were exposed to standard chow and a HFD during metabolic assessment or standard chow, water and 2% sucrose for sucrose preference.

Immunohistochemistry

Colonic, pancreatic, enteric, nodose and dorsal root ganglia tissues were fixed in 4% paraformaldehyde (PFA), dehydrated in 15% and 30% sucrose, and frozen in OCT embedding media (CellPath, Newtown, U.K.). Cryostat-cut sections (8-10µm) were mounted directly onto poly-L-lysine-covered glass slides (VWR, Leuven, Belgium) by the Institute of Metabolic Science Histology Core, except for nodose and dorsal root ganglia, which were cryosectioned at 6µm. Slides were incubated for 1hr in blocking solution containing 10% goat or donkey serum. Slides were stained overnight at 4^{o}C with primary antisera (table 1) in PBS/0.05% Triton X-100/10 % serum. Slides were washed with blocking solution and incubated with appropriate secondary antisera (donkey or goat Alexa Fluor® 488, 546, 555, 633 or 647; Invitrogen) diluted 1:400 and Hoechst diluted 1:1500 for 1 hr. Control sections were stained with secondary antisera alone. Sections were mounted with Prolong Gold (Life Technologies) or hydromount (National Diagnostics, Atlanta, Georgia, USA) prior to confocal microscopy (Leica TCS SP8 X, Wetzlar, Germany). Quantification of cell number was performed using Leica Application Suite X and Image J.

Brain tissue was collected from perfusion fixed mice as previously described [63]. Animals were anaesthetised with dolethal sodium pentobarbital solution at 125 mg/kg ip (in saline) and transcardially

perfused with heparinised 0.1M phosphate buffered saline (1xPBS) followed by 4% PFA in PBS. Brains were extracted and post-fixed in 4% PFA for 24 hrs at 4°C then transferred to 30% sucrose solution at 4°C for 48 hrs. Brains were sectioned coronally from olfactory bulb to the spinomedullary junction at 25 µm using a freezing microtome and stored in cryoprotectant medium. For diaminobenzidine (DAB) staining, antigen retrieval was used for all experiments prior to antibody incubation. Sections were incubated in 10 mM sodium citrate (Alfa Aesar, A12274) at 80°C for 10 minutes then washed in PBS. Sections were incubated in 0.5% hydrogen peroxide (Sigma, H1009) in milliQ water for 15 minutes then washed in PBS. Sections were blocked with 5% donkey serum in 0.3% Tween20 (VWR, 437082Q) in PBS (PBST) for 1 hr at room temperature, then incubated with GFP antiserum (1:4000; ab5450, Abcam) in blocking solution overnight at 4°C. After washing in 0.1% PBST, sections were incubated with biotinylated anti-goat IgG (1:400; AP180B, Millipore) in 0.3% PBST for 1.5 hrs at room temperature, followed by a 1 hr incubation with streptavidin conjugated to horseradish peroxidase (Vectastain Elite ABC kit, Vector Laboratories, PK-6100) and developed by DAB substrate (Abcam, ab94665). Sections were washed in PBS, prior to dehydration in ethanol and xylene, then mounting/coverslipping with Pertex mounting medium (Pioneer Research Chemicals Ltd., PRC/R/750). For immunofluorescent staining, slices were washed in PBS, prior to blocking for 1 hr in 5% donkey serum then incubation with primary antisera (table 1) in blocking solution overnight at 4°C. Slices were washed in and incubated with the appropriate secondary antisera (Alexa Fluor® 488 or 555; Invitrogen) diluted 1:500 for 2 hrs at room temperature. Following washing, mounted sections were coverslipped on superfrost slides using Vectashield (Vector Laboratories, H-1400-10). Slides were imaged using an Axio Scan.Z1 slide scanner (Zeiss) and confocal microscope (Leica TCS SP8 X, Wetzlar, Germany) with a 20x or 40x objective as indicated. Images were analysed in Halo Image Analysis Software (Indica Labs) and ImageJ.

Antigen	Raised In	Concentration	Source

GFP	Goat	1:1000 (unless specified)	Abcam, 5450
DSRed (RFP and mCherry)	Rabbit	1:1000	Takara Bio Clontech, 632496
Serotonin (5-HT)	Rabbit	1:10,000	Immunostar, 20080
Somatostatin	Rabbit	1:1000	Dako, A0566
Insulin	Guinea pig	1:100	Abcam, 7842
Glucagon	Rabbit	1:200	Santa Cruz, sc-7782
nNos	Goat	1:500	Abcam, 1376
Calretinin	Goat	1:300	Swant, cg1
NeuN	Mouse	1:1000	Millipore, MAB377

Table 1. Primary antisera used for immunohistochemistry.

Tissue extraction and reverse transcription-quantitative polymerase chain reaction (RT-qPCR)

Animals were culled by cervical dislocation. Brain and colon tissues were extracted and frozen immediately on dry ice. Nodose and dorsal root ganglia (colon innervating T11, T12, L1m L5, L6 and S1, located using the most caudal rib joint to the spine) were frozen on dry ice immediately after dissection and pooling in 2mL Eppendorf tubes. For pancreatic islet extraction, pancreases were injected with collagenase V (0.5 mg/ml) and digested at 37°C. Islets were hand-picked into HBSS containing 0.1% wt/vol. fatty acid-free BSA. Each pancreas yielded approximately 150–300 islets which were pooled.

RNA from whole tissue segments was extracted using TRI Reagent (Sigma, T9424) according to manufacturer's instructions. RT-qPCR was performed and analysed as described in [64] using probes *Rxfp4*: Mm00731536_s1 and *β-actin*: Mm02619580_g1 (Applied Biosytems). Mean, SEM and statistics were obtained for the ΔCT data and converted to relative expression levels ($2^{\Delta CT}$) for presentation only.

Dissociation, fluorescence-activated cell sorting (FACS) and single cell RNA sequencing

For large intestine epithelial cell samples, single cell suspensions were prepared from four *Rxfp4*-Cre731 x Rosa26-EYFP mice (biological replicates) as previously described with the outer muscle layer removed prior to processing [64]. Cells were separated by flow cytometry using a MoFlo Beckman Coulter Cytomation sorter (Coulter Corp., Hialeah, FL) at the Cambridge Institute for Medical Research (CIMR) Flow Cytometry Core Facility. Cell gating was set according to cell size (FSC), cell granularity (SSC), FSC pulse-width for singlets, fluorescence at 488 nm/532 nm for EYFP and 647/670 nm for nuclear stain with DraQ5 (Biostatus, Shepshed, Leicester, UK) to exclude cellular debris, aggregates and dead cells. All yellow fluorescent protein (YFP)-positive cells, and 20,000 negative cells, were collected separately into aliquots of 500 µL of buffer RLT+ (Qiagen), with 143 mmol/L β-mercaptoethanol. RNA was extracted using a RNeasy Micro plus kit (Qiagen) and quantified using an Agilent 2100 Bioanalyser. Sequencing and analysis were performed as previously described [65].

For hypothalamic samples, single cell suspensions were prepared and pooled from twelve female *Rxfp4*-Cre x EYFP mice (biological replicates) as previously described [63]. Briefly, mice were sacrificed by cervical dislocation and the hypothalamus dissected into Hibernate-A medium (ThermoFisher, A1247501) supplemented with 0.25% GlutaMAX (ThermoFisher, 35050061) and 2% B27 (ThermoFisher, A1895601). Tissue digested in Hibernate-A medium without calcium (BrainBits) containing 20 U/mL Papain (Worthington) and 1% GlutaMAX for 30 min at 37°C under agitation (Thermomixer, 500 rpm). After digestion, tissue was triturated in Hibernate-A medium with 3.5 U/mL DNase I (Sigma, D4263). The trituration supernatant was loaded on top of a BSA gradient prepared in Hibernate-A medium, spun for 5 min at 300 rcf, and the pellet was resuspended in Hibernate-A medium + 1% BSA. The cell suspension was filtered through a 70 µm cell strainer into a fresh tube. Fluorescence-activated cell sorting was performed using an Influx Cell Sorter (BD Biosciences, San Jose, CA, USA). Cell gating was set as above. Cells were sorted directly into individual wells of 96-well plates containing lysis buffer. 384 YFP-positive cells were isolated and processed using a Smart-Seq2 protocol [66]. Libraries were prepared from ~150 pg of DNA

using the Nextera XT DNA preparation kit (Illumina, FC-131-1096) and Nextera XT 96-Index kit (Illumina, FC-131-1002). Pooled libraries were run on the Illumina HiSeq 4000 at the Cancer Research UK Cambridge Institute Genomics Core. Sequencing reads were trimmed of adapters, aligned to the *Mus musculus* genome (GRCm38, Ensembl annotation version 101) using STAR (v2.7.3a), and raw counts generated using FeatureCounts (Subread v2.0.0). Downstream analyses were performed using the Seurat R package (v4.0.1). Samples were included in the final analyses only if they met all of the following criteria: (a) unique reads > 50%, (b) reads assigned to exons > 20%; (c) number of genes with (FPKM>1) > 3000; (d) total number of unique genes > 200. Genes were included in the final analyses if they were detected in at least 3 samples. Marker genes were identified for clusters using the FindAllMarkers function in the Seurat package; the top 20 gene markers were cross referenced against other bulk and single cell RNAseq databases to assign cell type. Neuronal clusters were identified in a similar fashion using appropriate marker genes.

RNAscope

Detection of Mouse *Rxfp4* was performed on fixed, frozen sections using Advanced Cell Diagnostics (ACD) RNAscope® 2.5 LS Reagent Kit-RED (Cat No. 322150), RNAscope® LS 2.5 Probe- Mm-Rxfp4 (Cat No. 317588) (ACD, Hayward, CA, USA). To prepare the sections, animals were anaesthetized with sodium pentobarbital solution (50 mg/kg in saline) and transcardially perfused with PBS followed by 4% PFA in PBS. Brains were extracted and post-fixed in 4% PFA for 24 hrs before being transferred to 25% sucrose for 24 hrs at 4°C. Brains were embedded in OCT compound, frozen in a Novec 7000 (Sigma)/dry ice slurry and stored at -80 C. 16μm cryosections containing the hypothalamus were prepared on a Leica CM1950 cryostat (Wetzlar, Germany) at -12°C and stored at -20°C until required.

Slides were thawed at room temperature for 10 min before baking at 60°C for 45 min. The sections were then post-fixed in pre-chilled 4% PFA for 15 min at 4°C, washed in 3 changes of PBS for 5 min each before dehydration through 50%, 70%, 100% and 100% ethanol for 5 min each. The slides were air-dried for 5 min before loading onto a Bond Rx instrument (Leica Biosystems). Slides were prepared using the frozen slide delay prior to pre-treatments using Epitope Retrieval Solution 2 (Cat No. AR9640, Leica Biosystems) at 95°C for 5 min, and ACD Enzyme from the LS Reagent kit at 40°C for 10 minutes. Probe hybridisation and signal amplification were performed according to manufacturer's instructions, with the exception of increased Amp5 incubation time at 30 min. Fast red detection of mouse *Rxfp4* was performed on the Bond Rx using the Bond Polymer Refine Red Detection Kit (Leica Biosystems, Cat No. DS9390) with an incubation time of 20 min. Slides were then removed from the Bond Rx and were heated at 60°C for 1 hr, dipped in xylene and mounted using EcoMount Mounting Medium (Biocare Medical, CA, USA. Cat No. EM897L). Sections were imaged on a Slide Scanner Axio Scan.Z1 microscope (Zeiss) using a 40x air objective. Three z-stack slices spanning 1.5µM were combined into an extended depth of field image (ZEN 2.6, Zeiss). The CZI files were read into Halo Image Analysis Software (Indica Labs).

Statistical analysis

All data were plotted using GraphPad Prism 7/8/9 software (GraphPad Software, Inc). Statistical analysis was performed by paired Student's t-tests, one-way ANOVA with multiple comparisons or two-way ANOVA with multiple comparisons, as indicated. N represents biological replicates. Sample size was computed based on pilot data and previously published data. Data are presented as mean ± SEM and probabilities of $p<0.05$ were considered statistically significant in all tests.

Acknowledgements

552 Metabolic Research Laboratories support was provided by the following core facilities: Disease Model
553 Core, Genomics and Transcriptomics Core, Histology Core, Imaging Core, and Core Biochemical Assay
554 Laboratory (supported by the MRC [MRC_MC_UU_12012/5] and Wellcome Trust [100574/Z/12/Z]). RNA-
555 sequencing was undertaken at the CRUK Cambridge Institute Genomics Core. Cell sorting was performed
556 at the NIHR Cambridge BRC Cell Phenotyping Hub. We thank the Histopathology/ISH Core Facility at
557 Cancer Research UK- Cambridge Institute, for assistance with in situ hybridisation. We also would like to
558 thank Chris Riches and Maša Josipović for initial help with metabolic and operant cages, Pierre Larraufie
559 for help with the EC transcriptome analysis and Van Lu for the help in the collection of nodose and dorsal
560 root ganglia. JAT is supported by a NIHR Clinical Lectureship (CL-2019-14-504). Research in the laboratory
561 of F.M.G. and F.R. is supported by the MRC (MRC_MC_UU_12012/3) and Wellcome Trust (106262/Z/14/Z
562 and 106263/Z/ 14/Z). O.R.M.W. is supported by an iCASE PhD studentship with AZ. F.M.G. and F.R. act as
563 guarantors for this manuscript.

564

565

566

567 **Author contributions**

568 JEL, ORMW, FMG and FR designed the research studies. JEL, ORMW, CB, LB and AEA conducted
569 experiments. SJK and BG conducted the SmartSeq2 protocol and library preparation for single-cell RNA-
570 sequencing and CAS led the bioinformatic analysis. EC and MT provided the rabies and AAV-helper viruses
571 for retrograde viral tracing. JAT prepared the tissues and gave guidance for RNAscope.DH and DB co-
572 supervised ORMW and BVP helped with the initial behavioural cage experiments. FR developed the
573 transgenic models. JEL, ORMW, FMG and FR wrote the manuscript. All authors revised the final draft.

574

575 **Competing interests**

F.M.G. is a paid consultant for Kallyope, New York. The Gribble-Reimann lab currently hosts projects that receive funding from AstraZeneca (O.R.M.W., BBSRC-iCase), Eli Lilly & Company and LGC. DH and DB are AZ employees and CB and BUP have also joined AZ since contributing to this work.

References

1. Bathgate, R.A. *et al.* Relaxin family peptides and their receptors. *Physiol Rev* **93**, 405-480 (2013).
2. Ang, S.Y. *et al.* The actions of relaxin family peptides on signal transduction pathways activated by the relaxin family peptide receptor RXFP4. *Naunyn Schmiedebergs Arch Pharmacol* **390**, 105-111 (2017).
3. Liu, C. & Lovenberg, T.W. Relaxin-3, INSL5, and their receptors. *Results Probl Cell Differ* **46**, 213-237 (2008).
4. Billing, L.J. *et al.* Co-storage and release of insulin-like peptide-5, glucagon-like peptide-1 and peptideYY from murine and human colonic enteroendocrine cells. *Mol Metab* (2018).
5. Grosse, J. *et al.* Insulin-like peptide 5 is an orexigenic gastrointestinal hormone. *Proceedings of the National Academy of Sciences of the United States of America* **111**, 11133-11138 (2014).
6. DeChristopher, B. *et al.* Discovery of a small molecule RXFP3/4 agonist that increases food intake in rats upon acute central administration. *Bioorganic & medicinal chemistry letters* **29**, 991-994 (2019).
7. Burnicka-Turek, O. *et al.* INSL5-deficient mice display an alteration in glucose homeostasis and an impaired fertility. *Endocrinology* **153**, 4655-4665 (2012).
8. Liu, C. *et al.* Identification of relaxin-3/INSL7 as a ligand for GPCR142. *J Biol Chem* **278**, 50765-50770 (2003).
9. Boels, K. & Schaller, H.C. Identification and characterisation of GPR100 as a novel human G-protein-coupled bradykinin receptor. *Br J Pharmacol* **140**, 932-938 (2003).
10. Kay, R.G., Galvin, S., Larraufie, P., Reimann, F. & Gribble, F.M. Liquid chromatography/mass spectrometry based detection and semi-quantitative analysis of INSL5 in human and murine tissues. *Rapid Commun Mass Spectrom* **31**, 1963-1973 (2017).
11. Lee, Y.S. *et al.* Insulin-like peptide 5 is a microbially regulated peptide that promotes hepatic glucose production. *Mol Metab* **5**, 263-270 (2016).
12. Zaykov, A.N., Gelfanov, V.M., Perez-Tilve, D., Finan, B. & DiMarchi, R.D. Insulin-like peptide 5 fails to improve metabolism or body weight in obese mice. *Peptides* **120**, 170116 (2019).
13. Lewis, J.E. *et al.* Selective stimulation of colonic L cells improves metabolic outcomes in mice. *Diabetologia* **63**, 1396-1407 (2020).
14. Munro, J. *et al.* Relaxin polymorphisms associated with metabolic disturbance in patients treated with antipsychotics. *J Psychopharmacol* **26**, 374-379 (2012).
15. Jendryka, M. *et al.* Pharmacokinetic and pharmacodynamic actions of clozapine-N-oxide, clozapine, and compound 21 in DREADD-based chemogenetics in mice. *Sci Rep* **9**, 4522 (2019).
16. Musatov, S. *et al.* Silencing of estrogen receptor alpha in the ventromedial nucleus of hypothalamus leads to metabolic syndrome. *Proc Natl Acad Sci U S A* **104**, 2501-2506 (2007).
17. Luo, S.X. *et al.* Regulation of feeding by somatostatin neurons in the tuberal nucleus. *Science* **361**, 76-81 (2018).

18. Kim, D.W. *et al.* Multimodal Analysis of Cell Types in a Hypothalamic Node Controlling Social Behavior. *Cell* **179**, 713-728.e717 (2019).
19. van Veen, J.E. *et al.* Hypothalamic estrogen receptor alpha establishes a sexually dimorphic regulatory node of energy expenditure. *Nat Metab* **2**, 351-363 (2020).
20. Li, M.M. *et al.* The Paraventricular Hypothalamus Regulates Satiety and Prevents Obesity via Two Genetically Distinct Circuits. *Neuron* **102**, 653-667.e656 (2019).
21. Wall, N.R., Wickersham, I.R., Cetin, A., De La Parra, M. & Callaway, E.M. Monosynaptic circuit tracing in vivo through Cre-dependent targeting and complementation of modified rabies virus. *Proc Natl Acad Sci U S A* **107**, 21848-21853 (2010).
22. Mashima, H., Ohno, H., Yamada, Y., Sakai, T. & Ohnishi, H. INSL5 may be a unique marker of colorectal endocrine cells and neuroendocrine tumors. *Biochem Biophys Res Commun* **432**, 586-592 (2013).
23. Thanasupawat, T. *et al.* INSL5 is a novel marker for human enteroendocrine cells of the large intestine and neuroendocrine tumours. *Oncol Rep* **29**, 149-154 (2013).
24. Luo, X. *et al.* The insulinotrophic effect of insulin-like peptide 5 in vitro and in vivo. *Biochem J* **466**, 467-473 (2015).
25. Adriaenssens, A.E. *et al.* Transcriptomic profiling of pancreatic alpha, beta and delta cell populations identifies delta cells as a principal target for ghrelin in mouse islets. *Diabetologia* **59**, 2156-2165 (2016).
26. Ewbank, S.N. *et al.* Chronic G. *Proc Natl Acad Sci U S A* **117**, 20874-20880 (2020).
27. King, B.M. The rise, fall, and resurrection of the ventromedial hypothalamus in the regulation of feeding behavior and body weight. *Physiol Behav* **87**, 221-244 (2006).
28. MILLER, N.E., BAILEY, C.J. & STEVENSON, J.A. Decreased "hunger" but increased food intake resulting from hypothalamic lesions. *Science* **112**, 256-259 (1950).
29. TEITELBAUM, P. Random and food-directed activity in hyperphagic and normal rats. *J Comp Physiol Psychol* **50**, 486-490 (1957).
30. Grossman, S.P. The

VMH: a center for affective reactions, satiety, or both? . **1**, 1-10 (1966).
31. Lindberg, D., Chen, P. & Li, C. Conditional viral tracing reveals that steroidogenic factor 1-positive neurons of the dorsomedial subdivision of the ventromedial hypothalamus project to autonomic centers of the hypothalamus and hindbrain. *J Comp Neurol* **521**, 3167-3190 (2013).
32. Hashikawa, K. *et al.* Esr1. *Nat Neurosci* **20**, 1580-1590 (2017).
33. Coutinho, E.A. *et al.* Activation of SF1 Neurons in the Ventromedial Hypothalamus by DREADD Technology Increases Insulin Sensitivity in Peripheral Tissues. *Diabetes* **66**, 2372-2386 (2017).
34. Viskaitis, P. *et al.* Modulation of SF1 Neuron Activity Coordinately Regulates Both Feeding Behavior and Associated Emotional States. *Cell Rep* **21**, 3559-3572 (2017).
35. Yang, C.F. *et al.* Sexually dimorphic neurons in the ventromedial hypothalamus govern mating in both sexes and aggression in males. *Cell* **153**, 896-909 (2013).
36. Lee, H. *et al.* Scalable control of mounting and attack by Esr1+ neurons in the ventromedial hypothalamus. *Nature* **509**, 627-632 (2014).
37. Krause, W.C. & Ingraham, H.A. Origins and Functions of the Ventrolateral VMH: A Complex Neuronal Cluster Orchestrating Sex Differences in Metabolism and Behavior. *Adv Exp Med Biol* **1043**, 199-213 (2017).
38. Correa, S.M. *et al.* An estrogen-responsive module in the ventromedial hypothalamus selectively drives sex-specific activity in females. *Cell Rep* **10**, 62-74 (2015).
39. Ebling, F.J.P. & Lewis, J.E. Tanycytes and hypothalamic control of energy metabolism. *Glia* **66**, 1176-1184 (2018).

40. Rogge, G., Jones, D., Hubert, G.W., Lin, Y. & Kuhar, M.J. CART peptides: regulators of body weight, reward and other functions. *Nat Rev Neurosci* **9**, 747-758 (2008).
41. Cavuoto, P. & Wittert, G.A. The role of the endocannabinoid system in the regulation of energy expenditure. *Best Pract Res Clin Endocrinol Metab* **23**, 79-86 (2009).
42. Xu, B. *et al.* Brain-derived neurotrophic factor regulates energy balance downstream of melanocortin-4 receptor. *Nat Neurosci* **6**, 736-742 (2003).
43. Sampson, C.M. *et al.* Small-Molecule Neuromedin U Receptor 2 Agonists Suppress Food Intake and Decrease Visceral Fat in Animal Models. *Pharmacol Res Perspect* **6**, e00425 (2018).
44. Moon, Y.S. *et al.* Mice lacking paternally expressed Pref-1/Dlk1 display growth retardation and accelerated adiposity. *Mol Cell Biol* **22**, 5585-5592 (2002).
45. Wermter, A.K. *et al.* Preferential reciprocal transfer of paternal/maternal DLK1 alleles to obese children: first evidence of polar overdominance in humans. *Eur J Hum Genet* **16**, 1126-1134 (2008).
46. Wang, D. *et al.* Whole-brain mapping of the direct inputs and axonal projections of POMC and AgRP neurons. *Front Neuroanat* **9**, 40 (2015).
47. Williams, G. *et al.* The hypothalamus and the control of energy homeostasis: different circuits, different purposes. *Physiology & behavior* **74**, 683-701 (2001).
48. Kelley, A.E., Baldo, B.A., Pratt, W.E. & Will, M.J. Corticostriatal-hypothalamic circuitry and food motivation: integration of energy, action and reward. *Physiology & behavior* **86**, 773-795 (2005).
49. Kenny, P.J. Reward mechanisms in obesity: new insights and future directions. *Neuron* **69**, 664-679 (2011).
50. Tobiansky, D.J. *et al.* The medial preoptic area modulates cocaine-induced activity in female rats. *Behav Neurosci* **127**, 293-302 (2013).
51. Tryon, V.L. & Mizumori, S.J.Y. A Novel Role for the Periaqueductal Gray in Consummatory Behavior. *Front Behav Neurosci* **12**, 178 (2018).
52. Wu, Q., Boyle, M.P. & Palmiter, R.D. Loss of GABAergic signaling by AgRP neurons to the parabrachial nucleus leads to starvation. *Cell* **137**, 1225-1234 (2009).
53. Chiang, M.C. *et al.* Parabrachial Complex: A Hub for Pain and Aversion. *J Neurosci* **39**, 8225-8230 (2019).
54. Lo, L. *et al.* Connectional architecture of a mouse hypothalamic circuit node controlling social behavior. *Proc Natl Acad Sci U S A* **116**, 7503-7512 (2019).
55. Ma, S., Smith, C.M., Blasiak, A. & Gundlach, A.L. Distribution, physiology and pharmacology of relaxin-3/RXFP3 systems in brain. *Br J Pharmacol* **174**, 1034-1048 (2017).
56. Atasoy, D., Aponte, Y., Su, H.H. & Sternson, S.M. A FLEX switch targets Channelrhodopsin-2 to multiple cell types for imaging and long-range circuit mapping. *J Neurosci* **28**, 7025-7030 (2008).
57. Shimshek, D.R. *et al.* Codon-improved Cre recombinase (iCre) expression in the mouse. *Genesis* **32**, 19-26 (2002).
58. Srinivas, S. *et al.* Cre reporter strains produced by targeted insertion of EYFP and ECFP into the ROSA26 locus. *BMC Dev Biol* **1**, 4 (2001).
59. Zhu, H. *et al.* Cre-dependent DREADD (Designer Receptors Exclusively Activated by Designer Drugs) mice. *Genesis* **54**, 439-446 (2016).
60. Zariwala, H.A. *et al.* A Cre-dependent GCaMP3 reporter mouse for neuronal imaging in vivo. *J Neurosci* **32**, 3131-3141 (2012).
61. Luche, H., Weber, O., Nageswara Rao, T., Blum, C. & Fehling, H.J. Faithful activation of an extra-bright red fluorescent protein in "knock-in" Cre-reporter mice ideally suited for lineage tracing studies. *Eur J Immunol* **37**, 43-53 (2007).

62. Heath, C.J., Phillips, B.U., Bussey, T.J. & Saksida, L.M. Measuring Motivation and Reward-Related Decision Making in the Rodent Operant Touchscreen System. *Current protocols in neuroscience* **74**, 8.34.31-38.34.20 (2016).
63. Adriaenssens, A.E. *et al.* Glucose-Dependent Insulinotropic Polypeptide Receptor-Expressing Cells in the Hypothalamus Regulate Food Intake. *Cell metabolism* **30**, 987-996.e986 (2019).
64. Billing, L.J. *et al.* Single cell transcriptomic profiling of large intestinal enteroendocrine cells in mice - Identification of selective stimuli for insulin-like peptide-5 and glucagon-like peptide-1 co-expressing cells. *Molecular metabolism* **29**, 158-169 (2019).
65. Roberts, G.P. *et al.* Comparison of Human and Murine Enteroendocrine Cells by Transcriptomic and Peptidomic Profiling. *Diabetes* **68**, 1062-1072 (2019).
66. Picelli, S. *et al.* Smart-seq2 for sensitive full-length transcriptome profiling in single cells. *Nat Methods* **10**, 1096-1098 (2013).

Figure Legends

Figure 1: RXFP4 is expressed in the central nervous system.

a) Scaled schematic of the bacterial artificial chromosome used to make *Rxfp4*-Cre mice. b) Crossing of *Rxfp4*-Cre mice with GFP-based reporter mice (EYFP or GCaMP3) used to detect *Rxfp4* expression in Fig 1 through GFP immunohistochemistry. c) Representative section from the colon of RXFP4^{EYFP} mice demonstrating *Rxfp4* expression in epithelial cells. Scale bar = 100 um. d,e) Coronal section of RXFP4^{GCaMP3} mice show distinct *Rxfp4*-expressing cell clusters in the ventrolateral part of the ventromedial hypothalamus (VMHvl) and adjacent tuberal nucleus. Scale bars = 500 μm. f) Co-staining for DAPI (blue), GFP (green) and NeuN (red) in the VMHvl of RXFP4^{GCaMP3} mice. Scale bar = 100 μm. g,h) Coronal sections of C57Bl6 mice labelled for *Rxfp4* mRNA in the VMHvl using RNAscope. Scale bar = 1 mm and 50 μm in the enlarged image (h).

Suppl Fig1: Rxfp4 expression in peripheral tissues of interest

a) Co-localisation of GFP (green) and serotonin (red) in colonic epithelial cells from RXFP4^{EYFP} mice, with nuclei stained blue (Hoechst). Scale bar = 20 μm. a(i) Percentage of singly GFP and GFP/5-HT double positive cells in n=3 mice, with 6-8 images taken at x20 magnification per mouse. b) Heatmap showing the top 20 most differentially expressed genes found during RNA-sequencing of FACS-isolated cell populations from four RXFP4^{EYFP} mice large intestines (non-coding and mitochondrial genes were excluded). Values are log10(FPKM+1). Genes and samples are grouped via hierarchical clustering based on Euclidean distance and complete linkage. c) EYFP positive (+) and control (-) cell populations were generated by FACS from RXFP4^{EYFP} mouse large intestinal tissue (n=3). mRNA was extracted and expression of tryptophan hydroxylase 1 (*Tph1*), peptide YY (*Pyy*), proglucagon (*Gcg*), insulin-like peptide 5 (*Insl5*), vesicular monoamine transporter 1 (*VMAT1, Slc18a1*), glucagon-like peptide 1 receptor (*Glp1r*) and *Rxfp4* determined relative to β-actin. mRNA undetected (UD). Mean ΔCT and upper SEM were calculated and

748 data presented as 2^ΔCT. Statistically significant differences as indicated were assessed on the non-
749 transformed data using a two-way ANOVA and post hoc Bonferroni (effect of genotype [F(1,2)=101.8, p =
750 0.0097, *Tph1* p = <0.0001, *Pyy* <0.0001, *Gcg* 0.0001, *Insl5* 0.0002, *Scl18a1* < 0.0001, *Glp1r* < 0.0001 and
751 *Rxfp4* < 0.0001 respectively). d) Representative images from cultured colonic enteric ganglia from
752 RXFP4^{tdRFP} mice immunostained for (left) red fluorescent protein (RFP, green) and neuronal nitric oxide
753 synthase (nNOS, red), and (right) Calretinin (green) and RFP (red). No RFP presence was observed. Nuclei
754 stained with Hoechst (blue); Scale bar = 50 µm. e) Representative dorsal root and e) nodose ganglion from
755 RXFP4^{EYFP} mice stained with GFP (green) and Hoechst (blue) Scale bars = 200 µm. g,h) Representative
756 pancreatic islets sections from RXFP4^{EYFP} mice stained for GFP (green), insulin (Ins, white) and either
757 glucagon (Gcg, red (f) or somatostatin (Sst, red (g)); Nuclei stained by Hoechst (blue); No GFP-staining was
758 observed; scale bars = 20 µm. i) *Rxfp4* mRNA detected in different tissues by RT-qPCR (n=3 mice). Bars
759 represent mean $2^{\Delta CT}$± SEM compared to *β-actin*. NG = nodose ganglion, DRG (ci) = colon innervating dorsal
760 root ganglia, DRG = other dorsal root ganglia.

761 **Suppl. Fig 2: *Rxfp4* expression in the central nervous system**

762 Coronal sections from RXFP4^{GCaMP3} mice stained for GFP immunoreactivity reveal *Rxfp4* expression in
763 various central nuclei. Red circles represent the presence of immunoreactive cells. Reference images
764 based on the Paxinos Mouse Brain Atlas with the A/P coordinates from bregma indicated in the top left
765 corner. AOB: Accesory olfactory bulb; GrO: Granular cell layer of the olfactory; vn: vomeronasal nerve;
766 ACC: anterior cingulate cortex; SSC: somatosensory cortex; GI: granular insular cortex; SFi: septofimbrial
767 nucleus; TS: triangular septal nucleus; SFO: subfornical organ; NBD: nucleus of the diagonal band; AV:
768 anteroventral thalamic nucleus; AHA: anterior hypothalamic area; PLH: peduncular lateral hypothalamus;
769 PVH: paraventricular hypothalamus; MCPO: magnocellular preoptic nucleus; AA: anterior amygdaloid
770 area; SI: substantia innominata; GP: globus pallidus; RSC: retrosplenial cortex; MHb: medial habenular
771 nucleus; CeA: central amygdala; CoA: cortical amygdala; DEn: dorsal endopiriform nucleus; DMH:

dorsomedial hypothalamus; VMHvl: ventromedial hypothalamus ventrolateral part; ARC: arcuate nucleus; ZI: zona incerta; BLA: basolateral amygdala; DS: dorsal subiculum; SC: superior colliculus; PAG: periaqueductal grey (D: dorsal, L: lateral, VL: ventrolateral); scp: superior cerebellar peduncle; SuM: supramammillary nucleus; MM: medial mammillary nucleus; MnM: medial mammillary nucleus median part; LM: lateral mammillary nucleus; PMCoA: posteromedial cortical amydala; PnO: pontine reticular nucleus oral part; ml: medial lemniscus; lfp: longitudinal fasciculus of the pons; Cu: cuneate nucleus; Sp5: spinal trigeminal tract (C: caudal part, I: interpolar part).

Figure 2: CNO alters feeding and food preference in RXFP4$^{wb\text{-}Di}$ mice.

a) Schematic of RXFP4$^{wb\text{-}Di}$ mouse model. b-d) Food intake in RXFP4$^{wb\text{-}Di}$ mice of standard chow (t=0.5536, p = 0.5875) (b) or HFD (45%) (t=2.612, p = 0.0189) (c) or liquid Ensure (HPM) (t=2.648, p = 00175) (d) 1 hour post CNO/vehicle treatment at 11:00 (n = 17, paired two-tailed t test, animals adapted to the appearance of test meal over the course of two weeks). (e) 1st hr (effect of treatment [F(1,36)=14.86, p = 0.0005], std chow p = 0.7604, HFD p = 0.03, kcal p = 0.0121) and (f) 2nd hr food (effect of treatment [F(1,36)=2.219, p = 0.1450], std chow p = 0.9918, HFD p = 0.6691, kcal p = 0.4979) consumption after CNO (orange) or saline (black) injection at 11:00 (n = 7 , two-way ANOVA with Sidak's multiple-comparison test) when mice had a choice between chow or HFD.

Suppl. Fig 3: Calorimetric data from Rxfp4 Di and Dq mice

Ambulatory activity (a,c,e) and energy expenditure (b,d,f) of RXFP4$^{wb\text{-}Di}$ (a,b, effect of time [F(8.262, 115.7) = 2.092, p = 0.0402] and effect of time [F(11.52, 161.3) = 8.018, p < 0.0001] respectively), RXFP4$^{wb\text{-}Dq}$ (c,d, effect of time [F(3.934,55.08) = 1.610, p = 0.0137 and effect of treatment [F(1, 13) = 5.860, p = 0.0309) and RXFP4^{VMHDq} (e,f, effect of time [F(6.859, 82.31) = 4.411, p = 0.0004) and effect of time [F(4.170, 50.05) = 4.180, p = 0.0048) mice housed in metabolic cages in response to CNO (orange) or saline (black). Conditions and stats as in Fig2 (Di), Fig3 (Dq) and Fig5 (VMH-Dq), respectively.

Figure 3: CNO alters feeding and food preference in RXFP4$^{wb\text{-}Dq}$ mice

a) Schematic of RXFP4$^{wb\text{-}Dq}$ mouse model. b-d) Food intake of (b) standard chow (t=0.1.235, p = 0.2628) (c) HFD (45%) (t=5.136, p = 0.0021) and (d) liquid Ensure (HPM) (t=7.725, p = 0.0002) 1 hour post CNO/saline treatment at 19:00 (n = 7, paired two-tailed t test, animals adapted to the appearance of test meal over the course of two weeks). e) 1st hr (effect of treatment [F(1,42) = 13.17, p = 0.0008, std chow p = 0.9321, HFD p = 0.0377, kcal p = 0.0092) and f) 2nd hr (effect of treatment [F(1,36)=0.1177, p = 0.7335], std chow p = 0.9475, HFD p = 0.8197, kcal p = 0.9875) food consumption after CNO (orange) or saline (black) injection at 19:00 in mice housed in metabolic chambers (n = 7, two-way ANOVA with Sidak's multiple-comparison test). g-i) Performance parameters in mice trained in operant chambers when treated with CNO (orange) or vehicle (black): g) Number of rewards earned in FR5 (n = 12, t=6.874, p < 0.001, paired two-tailed t test). h) Breakpoint in PR4 (number of target responses emitted by an animal in the last successfully completed trial, before session termination or 60 min time-out) (n = 12, t=9.357, *** p < 0.001, paired two tailed t test). i) ERC performance post vehicle (black) or CNO (orange) treatment between 11-13:00 (n = 12, effect of treatment [F(1,44)=41.38, p < 0.0001, std chow p = 0.7212, HPM p < 0.0001, two-way ANOVA with Sidak's multiple-comparison test, animals calorically restricted to 95% BW).

Figure 4: Ventromedial hypothalamic *Rxfp4*-expressing neurons regulate food preference.

a) AAV-hM3Dq-mCherry was bilaterally injected into the ventromedial hypothalamus of *Rxfp4*-Cre mice. b) Targeting efficiency was confirmed post perfusion fixation. Representative image showing ARC, VMH and DMH, with only VMH demonstrating AAV-hMEDq-mCherry expression. c-e) Food intake of (c) standard chow (t=0.08018, p = 0.9387) (d) HFD (45%) (t=4.299, p = 0.0051) and (e) liquid Ensure (HPM) (t=5.140, 0.0021) 1 hour post CNO (orange) or vehicle (black) treatment at 19:00 (n = 7, paired two-tailed t test, animals adapted to the appearance of test meal over the course of two weeks. (f) 1st hr (effect of treatment [F(1,36)=13.86, p = 0.0007, std chow p = 0.8049, HFD p = 0.0008, kcal p = 0.008) and (g) 2nd hr (effect of treatment [F(1,36)=0.2153, p = 0.6454, std chow p = 0.9165, HFD p = 0.9971, kcal p = 0.9703)

819 food consumption of RXFP4^{VMHDq} mice post CNO (orange) or vehicle (black) treatment (n = 7 per group,
820 mean ± SEM). Scale bar = 50µm.

821 **Suppl. Fig 4: CNO does not alter sucrose preference in RXFP4^{VMHDq} mice.**

822 a) Water and sucrose (2%) intake of mice housed in metabolic cages in response to CNO (orange) or saline
823 (black) treatment (n = 7 per group, two-way ANOVA, effect of treatment [F(1,24)=0.09980, p = 0.7548]
824 with Sidak's multiple-comparison test, water p = 0.7582, 2% sucrose p = 0.9799).

825 **Figure 5: Transcriptomic profiling of hypothalamic *Rxfp4*-expressing cells by scRNAseq**

826 a,b) tSNE visualisation of 350 hypothalamic *Rxfp4*-expressing cells indicates five clusters (a). Cell types
827 were assigned according to the expression of a combination of canonical cell-type markers genes (b). The
828 red circle indicates the neuronal cluster used in further analysis. c) tSNE visualisation of the 95 neuronal
829 cells revealed seven sub-clusters. d) Violin plots showing expression of marker genes associated with
830 multiple neuronal cell types. All gene expression counts are log-normalised with scale-factor = 10^4.

831 **Suppl. Fig 5: Transcriptomic profiling of the neuronal cluster from scRNAseq of hypothalamic *Rxfp4*-**
832 **expressing cells**

833 Violin plots showing expression of multiple genes in the hypothalamic *Rxfp4*-expressing neuronal sub-
834 clusters. All gene expression counts are log-normalised with scale-factor = 10^4.

835 **Figure 6: Circuit mapping of hypothalamic *Rxfp4*-expressing cells**

836 a) Schematic illustrating unilateral microinjection of AAV8-DIO-hChR2(H134R)-mCherry into the VMHvl of
837 RXFP4^{GCaMP3} mice. b) Immunofluorescence images demonstrating co-localisation of GFP (green) and ChR2-
838 mCherry (red) starter cells in the target region at A/P -1.7mm from bregma. c) Representative images
839 showing ChR2-mCherry-immunoreactive axon terminals in various brain regions (n=3). For each image,
840 distance from bregma (in mm) is indicated at the bottom right. Scale bars = 100 um. 40x magnification. d)
841 Schematic illustrating unilateral microinjection of AVV2-TVAeGFP-oG into the VMHvl of *Rxfp4*-Cre mice

842 followed by a unilateral microinjection of Rab-ΔG-EnvA-mCherry 21 days later. e) Immunofluorescence
843 images demonstrating the colocalisation of GFP (green) and Rab-mCherry (red) starter cells in the target
844 region A/P -1.7mm from bregma. f) Representative immunofluorescence images showing Rab-mCherry-
845 immunoreactive cell bodies in various brain regions (n=3). For each image distance from bregma (in mm)
846 is indicated at the bottom right. 20x magnification. g) Schematic illustrating the regions positive for
847 anterograde projections (red arrows), retrograde projections (blue arrows) or bilateral projections (black
848 arrows) from RXFP4^{VMH} cells. Abbreviations: ARC: arcuate nucleus; BNST: bed nucleus of the stria
849 terminalis; POA: Preoptic area; CeA: central amygdala; LHA: lateral hypothalamic area; PVH:
850 paraventricular hypothalamus; VMHvl: ventromedial hypothalamus, ventrolateral part; PAG:
851 periaqueductal grey; PVT: paraventricular thalamic nucleus; PMN: premammillary nucleus.

852 **Suppl. Fig 6: Anterograde projection regions from RXFP4^{VMH} cells**
853 Representative images showing ChR2-mCherry-immunoreactive axon terminals in other brain regions,
854 further to those already indicated in Fig6 (n=3). For each image, distance from bregma (in mm) is indicated
855 at the bottom right. Scale bars = 100 um. 40x magnification. Abbreviations: AHA: anterior hypothalamic
856 area; EAC: extended amygdala central part; SI: substantia innominata; LHA: lateral hypothalamic area;
857 DMH: dorsomedial hypothalamus; VMHvl: ventromedial hypothalamus ventrolateral part; SuM:
858 supramammillary nucleus; LC: locus coeruleus; PMNd: premammillary nucleus dorsal part.

859 **Suppl. Fig 7: Chemogenetic manipulation of Rxfp4 expressing cells does not alter glucose tolerance**
860 IPGTT (2g/kg BW following 16hr fast) in a) RXFP4$^{wb\text{-}Di}$ (one-way ANOVA $F = 14.03$, $p = 0.0001$ with Tukey
861 multiple comparison lean – VEH vs lean – CNO $p = 0.9801$, DIO – VEH vs DIO – CNO $p = 0.9877$, lean VEH
862 vs DIO – VEH $p = 0.0021$ and lean – CNO vs DIO – CNO $p = 0.0018$) b) RXFP4$^{wb\text{-}Dq}$ (one-way ANOVA $F =$
863 16.57, $p < 0.0001$ with Tukey multiple comparison lean – VEH vs lean – CNO $p = 0.9779$, DIO – VEH vs DIO
864 – CNO $p = 0.9663$, lean VEH vs DIO – VEH $p = 0.0006$ and lean – CNO vs DIO – CNO $p = 0.0032$) mice kept

865 on a chow diet (lean) or after induction of diet induced obesity (DIO) after 16 weeks feeding of a 45% HFD.

866 (n = 3-7 per group).

867

868

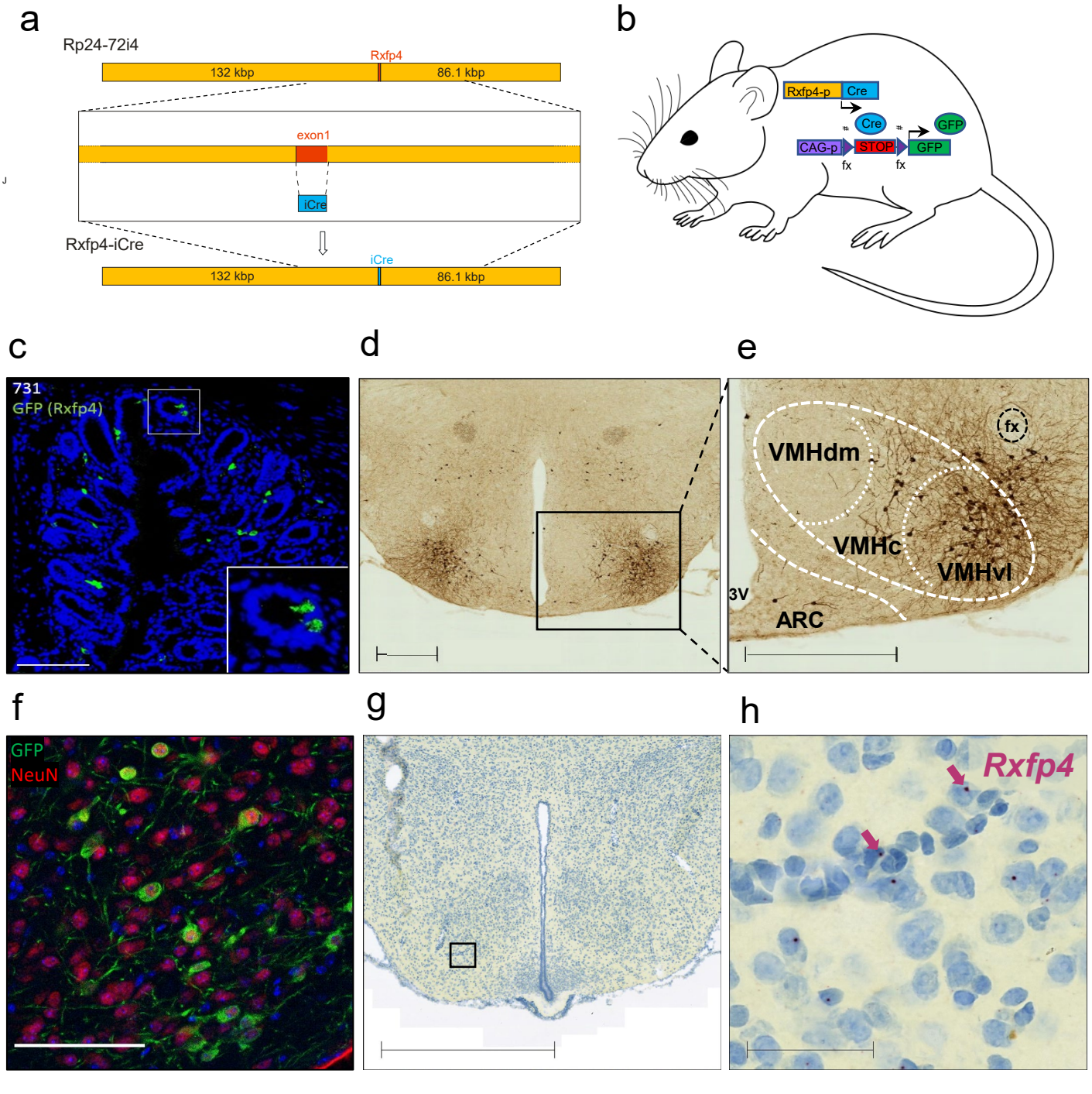

Figure 1

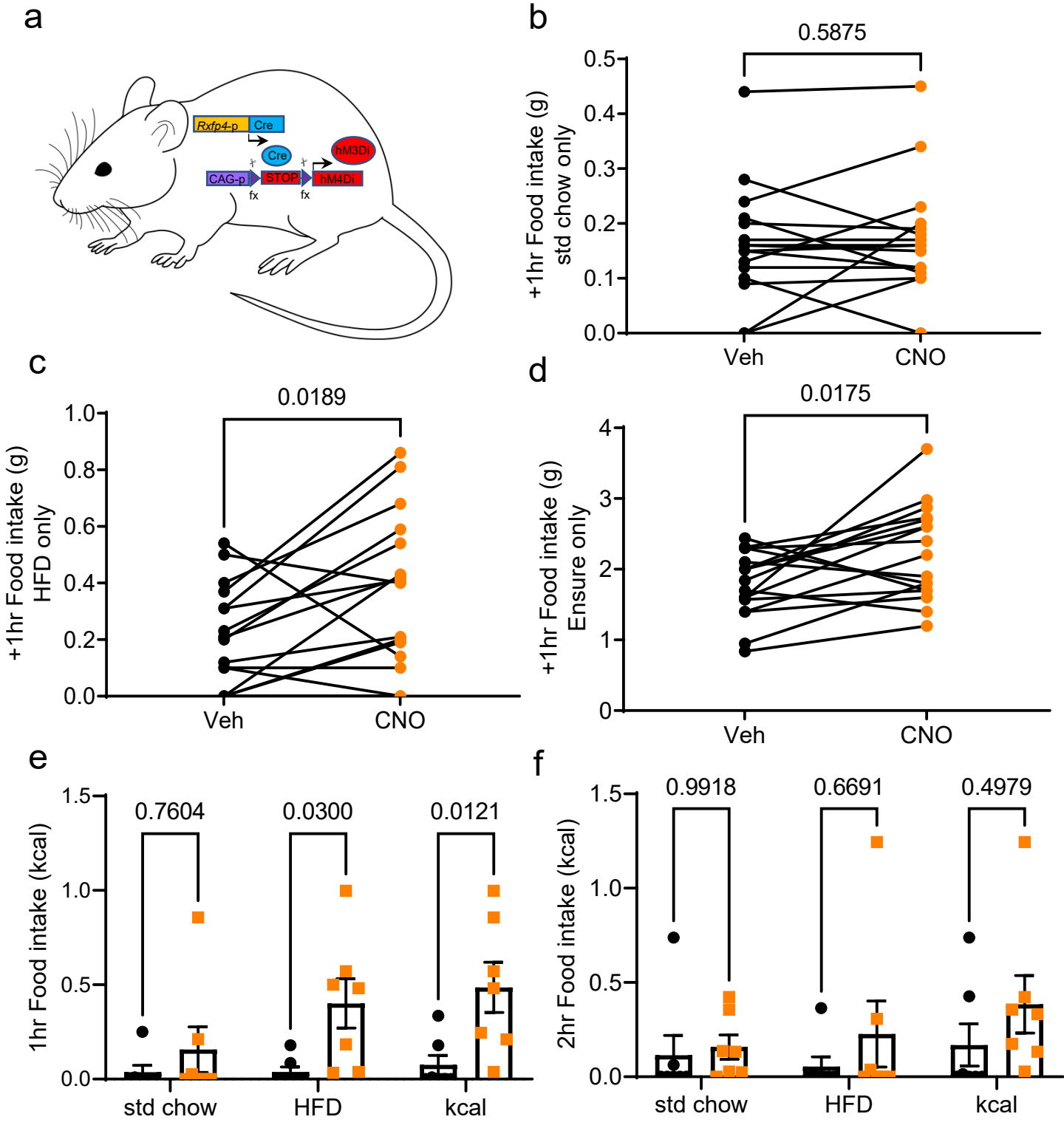

Figure 2

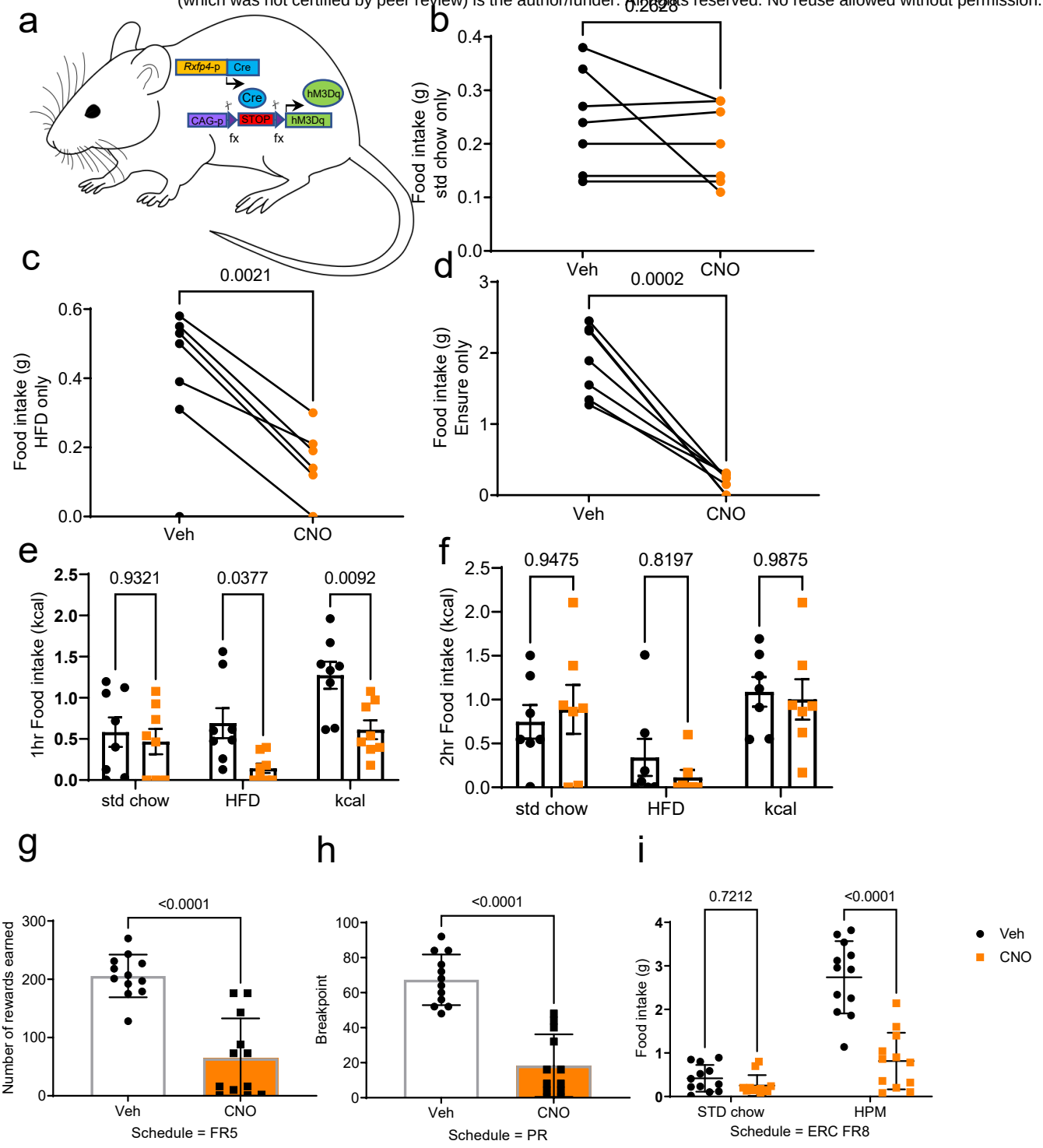

Figure 3

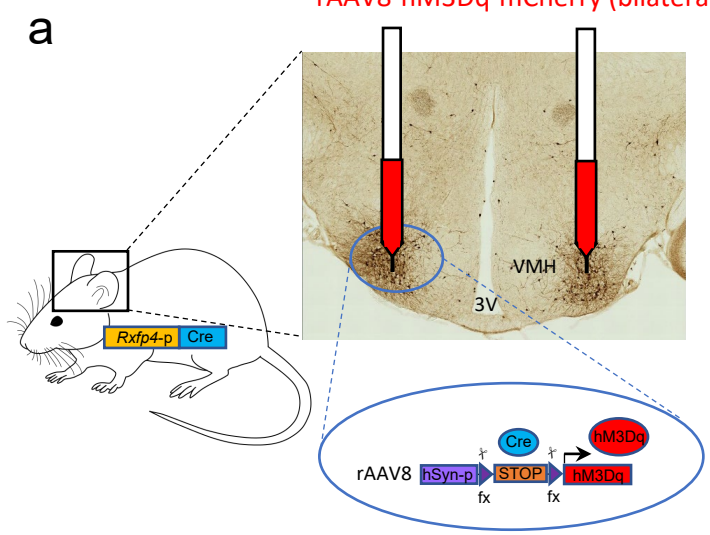

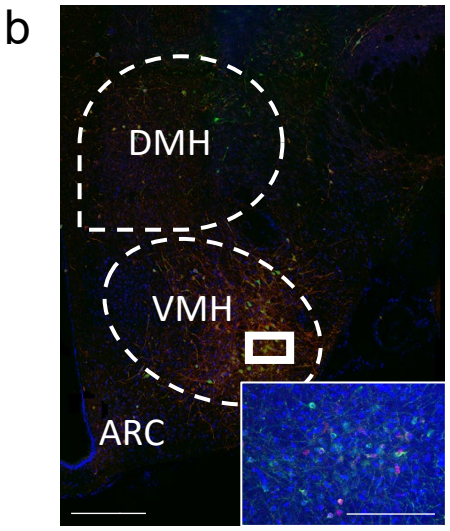

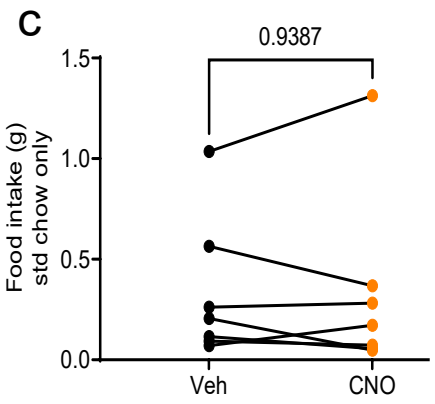

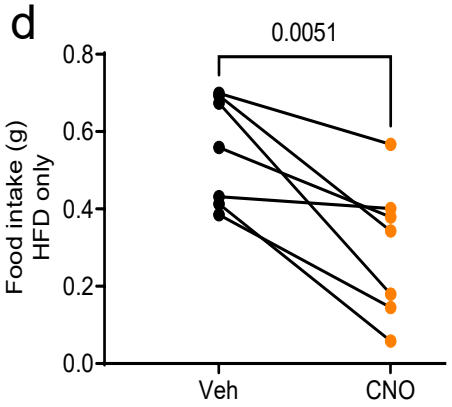

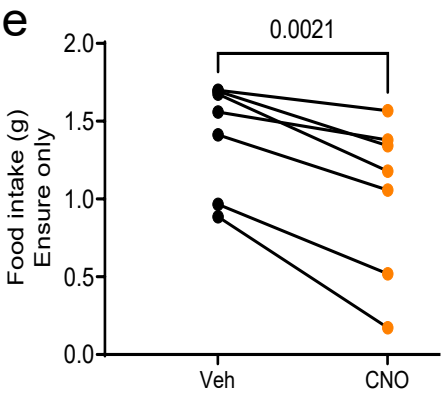

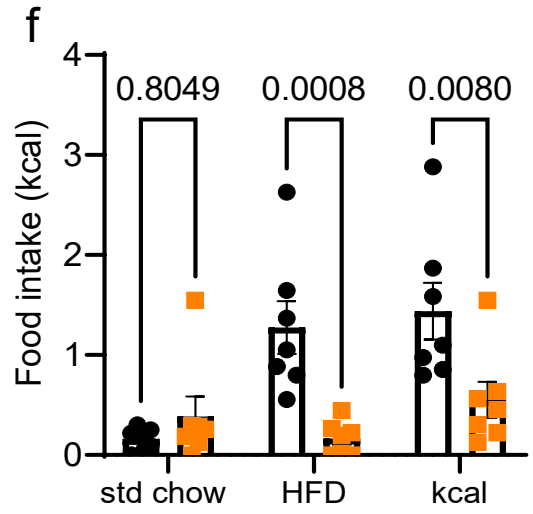

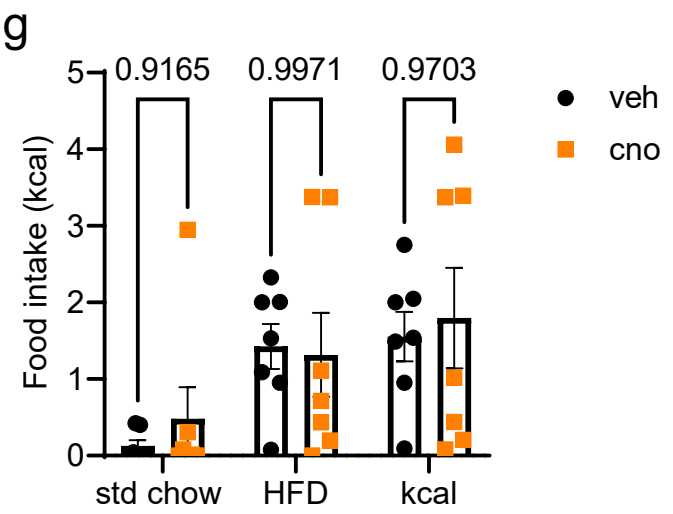

Figure 4

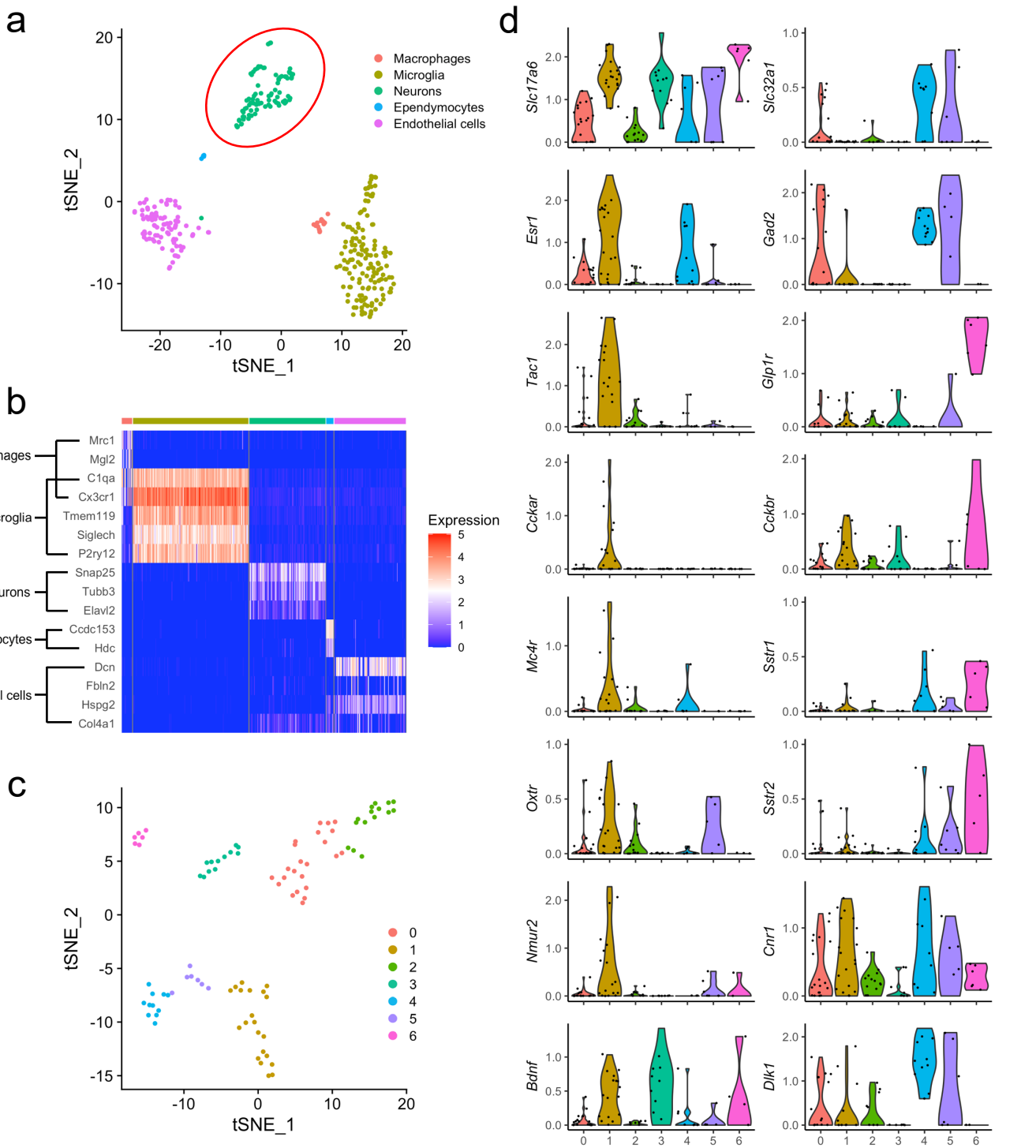

Figure 5

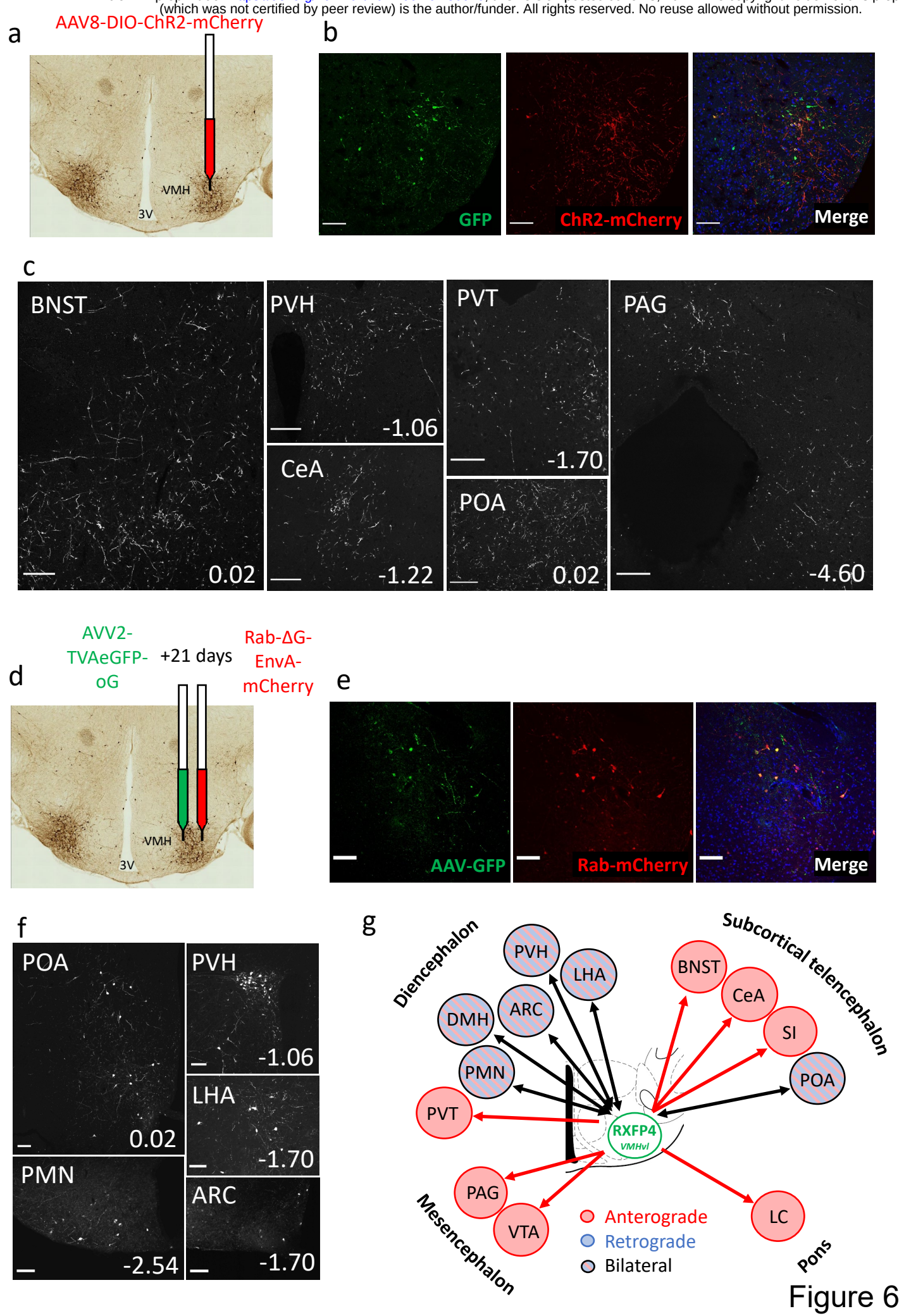

Figure 6